4

Substrate Integrated Coaxial Line based Three & Four port Networks

Microwave three-port and four-port passive components such as baluns, couplers, power dividers, and crossovers when fabricated using printed circuit board provides seamless integration across planar technologies and facilitates in building the system on substrate (SoS). Hence, reducing the over all size while simultaneously facilitating features such as wide-bandwidth and multi-band operation in microwave passive components remains a challenge for seamless integration with active circuits. In planar technologies, SICL stands out to serve the demanding requirements of the present communication standards. Owing to the mono-mode TEM mode propagation similar to its non-planar counterpart coaxial line, SICL can support non-dispersive wideband propagation with excellent electromagnetic compatibility. Further, SICL dual-band components operating at 6 GHz and 28 GHz targeted for 5G application are more preferable since implementation in microstrip or coplanar waveguide technology gives rise to radiation and surface loss at millimeter range & deteriorates the performance of the system. Moreover, problems like poor lateral shielding by stripline and SIW being not able to function in single mode to support dual-band operation for 5G standard is overcome by passive components implemented in SICL technology.

In this chapter, four different microwave passive components are implemented using SICL technology for wide-band/ multi-band operation.

1. **Baluns:**
   A. Design of wideband baluns for *K*-band application is explored using traditional and folded two-section branch-line balun SICL technology.
   B. A dual-band SICL balun operating at 6 GHz and 28 GHz for 5G application is realized using open-ended coaxial stubs with shielding. The performance of the dual-band SICL configuration is analyzed and range of realizable frequency ratios is determined from the analytically derived equations.
2. **Couplers:**
   A. A compact SICL based quadrature hybrid operating at 10 GHz specifically for *X*-band communication with controllable harmonic rejection is realized using four shielded open-ended coaxial stubs.
   B. Wide-band branch-line coupler using two cascaded sections of a single coupler is developed for K_u band to use in a six-port network.
   C. Miniaturized dual-broadband rat-race coupler operating simultaneously for *X*-Band and *K*-band with harmonic suppression up to 40 GHz is designed using short-circuited stubs in SICL technology.
3. **Crossover:**
   An SICL-based wideband crossover with low phase imbalance and group delay is designed for 0.2 to 20 GHz band. The proposed crossover due to its symmetric design provides low path difference without any additional phase compensation technique.
4. **Power-divider:**
   A two-stage Wilkinson power divider is realized in SICL technology operating over a wide-bandwidth covering 8 to 18 GHz. This passive network finds application in isolating the channels in a six-port module.

4.1 DESIGN OF SUBSTRATE INTEGRATED COAXIAL LINE WIDEBAND BALUN FOR *K*-BAND APPLICATIONS

In this section the design of substrate integrated coaxial line (SICL) based wideband baluns for *K*-band application is discussed. The proposed two-section branch-line balun realized in SICL technology can be fabricated using traditional PCB technology. The performance of the planar and folded balun are evaluated to demonstrate low amplitude and phase imbalance in the entire K-band covering 18 GHz to 26 GHz. The folded balun covers only 54.3% lateral area as compared to the planar balun. The wide-band single mode TEM characteristics of these baluns realized in SICL technology have enhanced shielding capability which motivates their usage in densely integrated millimeter-wave systems.

4.1.1 A two-section planar branch-line balun in SICL technology

The schematic of a two-section branch-line balun is depicted in Fig. 4.1. Balun is a three-port network that satisfies the following conditions:

$$|S_{ij}| = |S_{ji}| \tag{4.1}$$

where i, j = 1, 2, and 3, i ≠ j

$$S_{21} = -S_{31} \tag{4.2}$$

The proposed planar SICL based balun consists of two cascaded sections of conventional branch-line balun to achieve wideband performance. The vertical arms are of electrical length

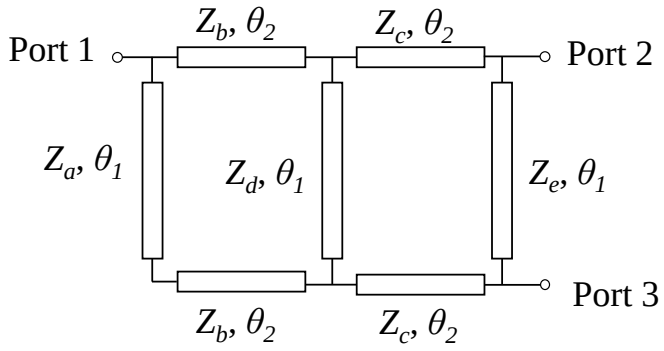

Figure 4.1 : Schematic of a two-section branch-line balun.

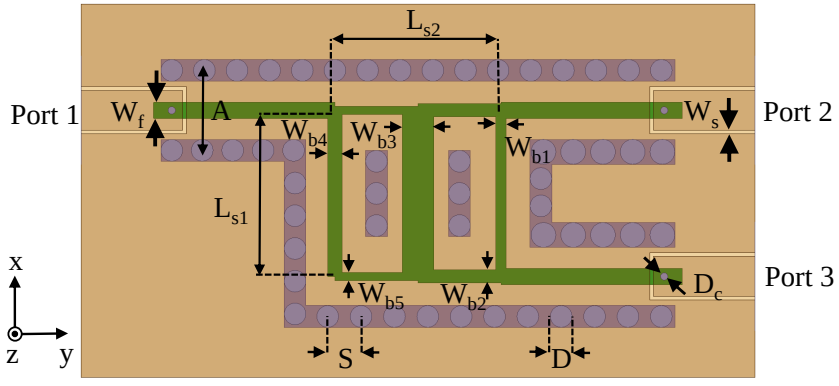

Figure 4.2 : Final layout of the proposed SICL based wideband balun.

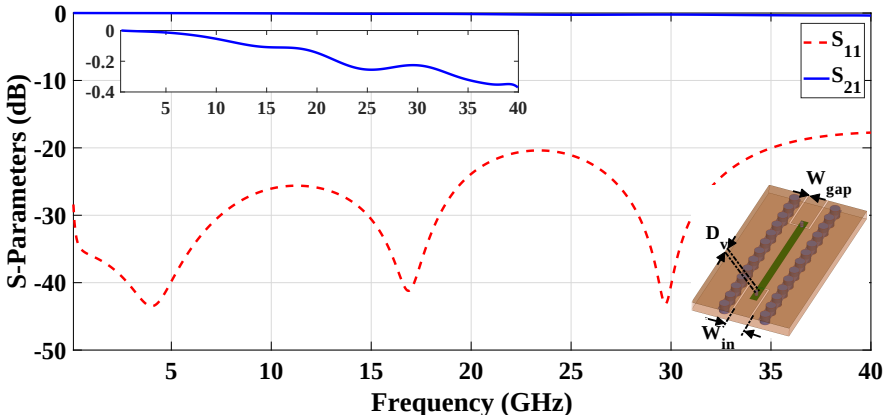

Figure 4.3 : Performance of the back to back SICL-GCPW transition.

θ_1 and each horizontal arm is of electrical length θ_2, where $\theta_1 = 180°$ and $\theta_2 = 90°$ with impedances as shown in Fig. 4.2. The entire configuration is laterally delimited by rows of metalized-vias. The diameter of via is D, spacing between vias is S and distance between rows of vias is A. Appropriate choice of the parameters namely D, A and S enables the designer to ensure single-mode TEM propagation throughout the band of operation [51]. The impedances of all the arms of two-section balun are optimized to satisfy (4.1) and (4.2) over a wide range of frequencies. The circuit parameters are given as Z_a = 52.9 Ω, Z_b = 74.1 Ω, Z_c = 56.7 Ω, Z_d = 56.7 Ω, and Z_e = 66.1 Ω [114]. The required characteristic impedance of SICL is realized by selecting the appropriate width of inner conducting strip and outer conductor by using the equation (2.9). The top-view of the final layout of the proposed SICL based wideband balun is presented in Fig. 4.2. As the proposed SICL based balun is the printed from of traditional coaxial line, it is expected to have low-dispersion and excellent ability to combat with electromagnetic interference in densely-packed systems. The proposed planar SICL based wideband balun is implemented by enclosing the inner conducting strip between Taconic TLY-5 (ε_r = 2.2, tanδ = 0.0009) substrate each of thickness 0.254 mm, which are bonded using Taconic FR-28 prepreg (ε_r = 2.74, tanδ = 0.0014). Since the inner conductor of SICL is not exposed, an SICL to GCPW transition is used for testing the prototype with a standard K-type connector. The designed transition demonstrates wide-band and low loss performance as shown

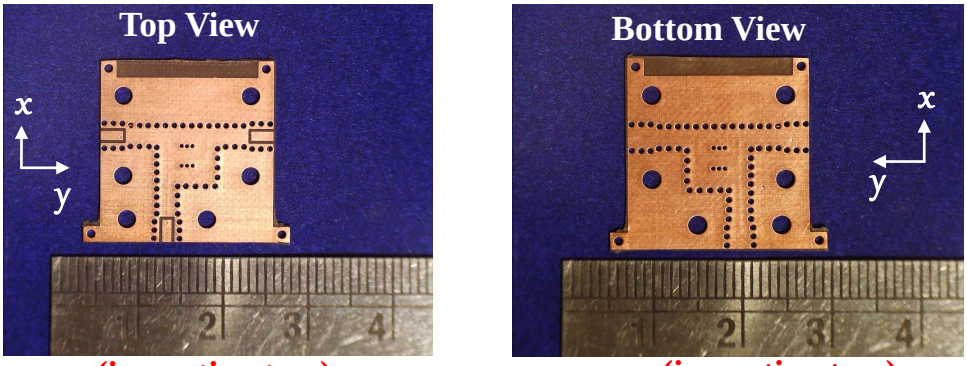

Figure 4.4 : Photograph of the fabricated wideband compact SICL balun for K-band applications (a) Top View (b) Bottom View

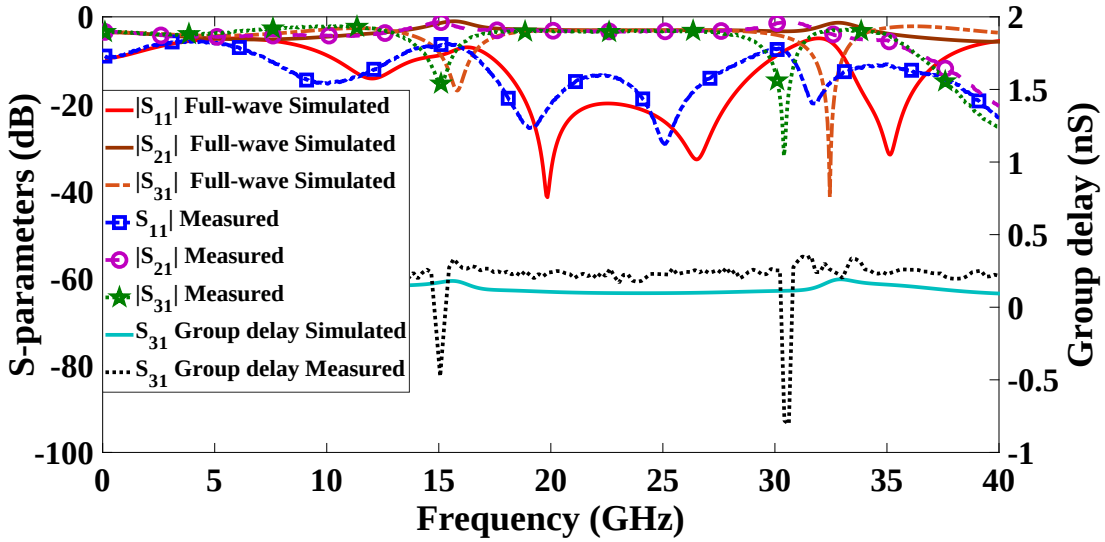

Figure 4.5 : Comparison between measured and and full-wave simulated S-parameters of planar wideband balun

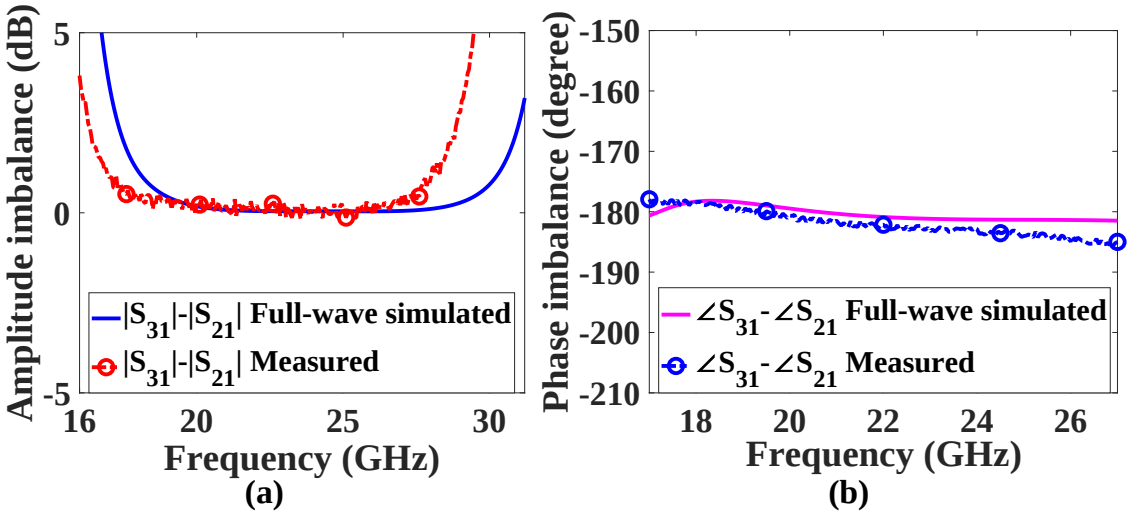

Figure 4.6 : Comparison between full-wave simulated amplitude and phase imbalance between output ports of the proposed planar SICL based wideband balun.

in Fig. 4.3 since a plated blind via hole in a thin substrate contributes to a very minor reactive component at higher frequencies. The SICL to GCPW transition designed with a total substrate height of 0.508 mm (Taconic TLY-5A) provides simulated insertion loss less than 0.4 dB and return loss better than atleast 20 dB up to 34 GHz. The performance of the proposed SICL based balun is evaluated using Ansys HFSS. An experimental prototype is fabricated using standard multilayer PCB technology. The photograph depicting the top and bottom view of the fabricated SICL based wideband SICL based balun is shown in Fig. 4.4.

4.1.2 Experimental validation of planar SICL based wideband balun

The fabricated experimental prototype of proposed planar SICL balun is tested with Agilent's N5234A (10 MHz to 43.5GHz) VNA. The full-wave simulated and measured S-parameters and the group-delay of the planar balun are shown in Fig. 4.5. The measured results indicate return loss better than 13 dB with amplitude and phase imbalance of the fabricated planar SICL balun better than ±0.3 dB and ±6° respectively in the frequency band covering 18 GHz to 26 GHz as shown in Fig. 4.6. The SICL based planar wideband balun covers 7.03 mm × 7.5 mm × 0.508 mm or equivalently $0.76\lambda_g \times 0.81\lambda_g \times 0.05\lambda_g$, where λ_g is guided wavelength at 22 GHz. The measured fractional bandwidth computed for the planar balun is 42.45% for an amplitude and phase imbalance of ±0.3 dB and ±4° respectively. The measured peak group delay of the fabricated SICL based planar balun 0.22 nsec at 22 GHz.

4.1.3 Multi-layer folded branch-line balun in SICL technology

The previously discussed design can be implemented in a smaller footprint by using a multi-layer configuration. A folded SICL based wideband balun is proposed using 4 substrate layers (Taconic TLY-5A (ε_r = 2.2, δ = 0.0009)) each of thickness 0.254 mm with 5 conducting layers. The top-view and the exploded view of the folded SICL balun are as shown in Fig. 4.7 & Fig. 4.8, respectively. One section of the proposed wideband balun is placed on the first substrate and the second section of the balun over the third layer of substrate which are separated by a dielectric substrate of same properties with thickness 0.254 mm. Two metallized vias connect both the sections that are folded over each other with a common ground plane. Slot of diameter W_c is cut in the middle ground plane to ensure isolation between the connecting vias and ground. The enlarged view of this configuration is shown in Fig. 4.8 and the dimensions are optimized to achieve wide-band response with minimal amplitude and phase imbalance. The dimensions of the proposed baluns are listed in Table 4.1.

4.1.4 Full-wave simulated performance of folded SICL based balun

The folded SICL based wideband balun for K-band is modeled and simulated in Ansys HFSS. The full-wave simulated S-parameters and the group-delay of the folded SICL balun shown

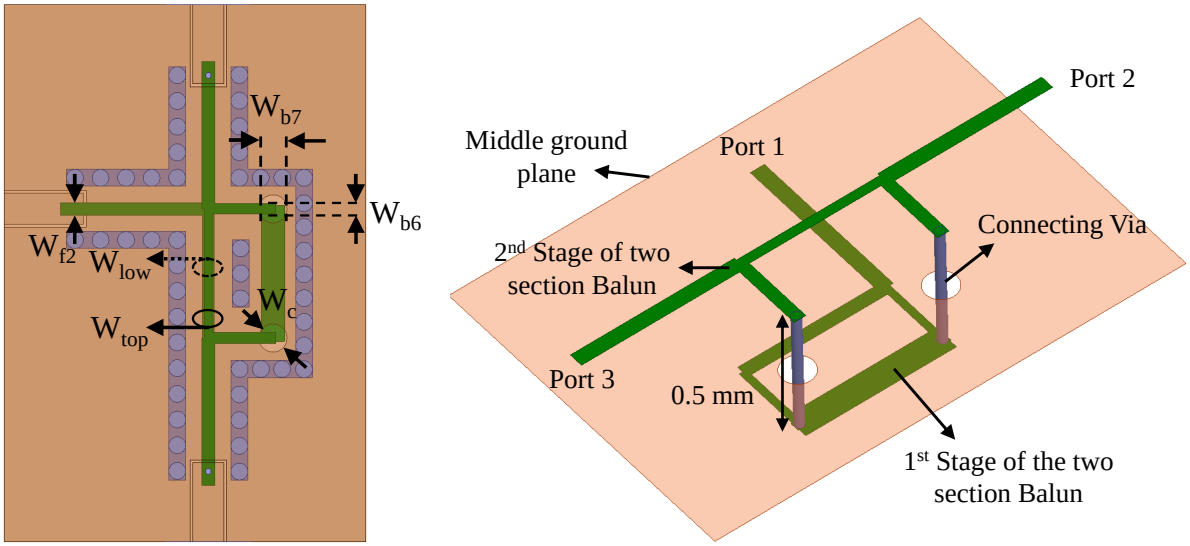

Figure 4.7 : Final layout of the proposed folded SICL based wideband balun a)Top-view b) Enlarged view

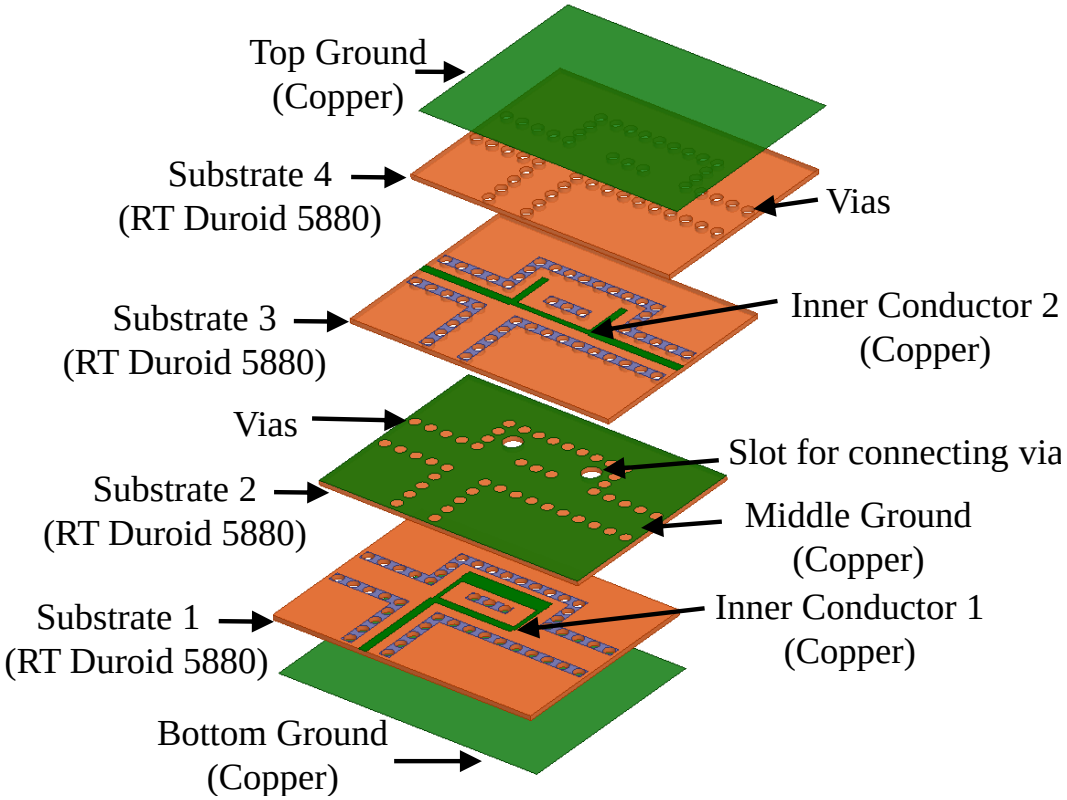

Figure 4.8 : Three-Dimensional view of the proposed folded SICL wideband balun.

Table 4.1 : Dimensions of the designed SICL based wideband baluns

Parameter	Value (mm)	Parameter	Value (mm)
W_{f_1}	0.44	L_{s1}	4.46
W_{f_2}	0.45	L_{s2}	4.92
W_{b_1}	0.28	S	0.9
W_{b_2}	0.36	D	0.6
W_{b_3}	0.87	D_c	0.15
W_{b_4}	0.4	W_{low}	0.42
W_{b_5}	0.22	W_{top}	0.29
W_{b_6}	0.37	W_{b_7}	0.83
W_s	0.1	W_c	1
A	2.4	D_v	0.15

in Fig. 4.9 indicates impedance matching better than 20 dB with equal power division at the output ports. As predicted, the folded SICL based balun demonstrates less than 0.2 ns group delay confirming SICL as a low-dispersive transmission media. From Fig. 4.10 simulated magnitude imbalance better than $|S_{21}| - |S_{31}| = \pm 0.4$ dB and $|S_{21}| - |S_{31}| = \pm 0.2$ dB is seen for the planar and folded version of SICL balun, respectively. Similarly, simulated phase imbalance better than $\angle S_{21} - \angle S_{31} = 1.7^\circ$ and $\angle S_{21} - \angle S_{31} = \pm 0.6^\circ$ have been observed for planar and folded SICL based baluns

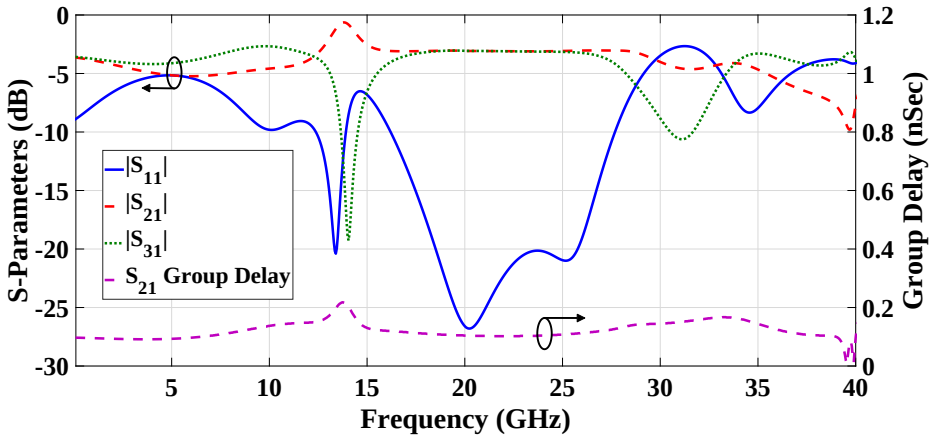

Figure 4.9 : Full-wave simulated S-parameters of proposed folded SICL based wideband balun

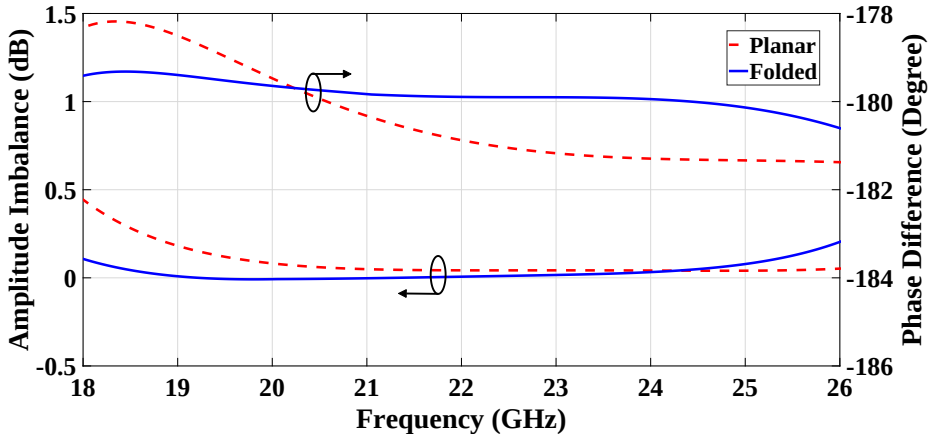

Figure 4.10 : Full-wave simulated magnitude and phase difference between output ports of the proposed planar and folded baluns.

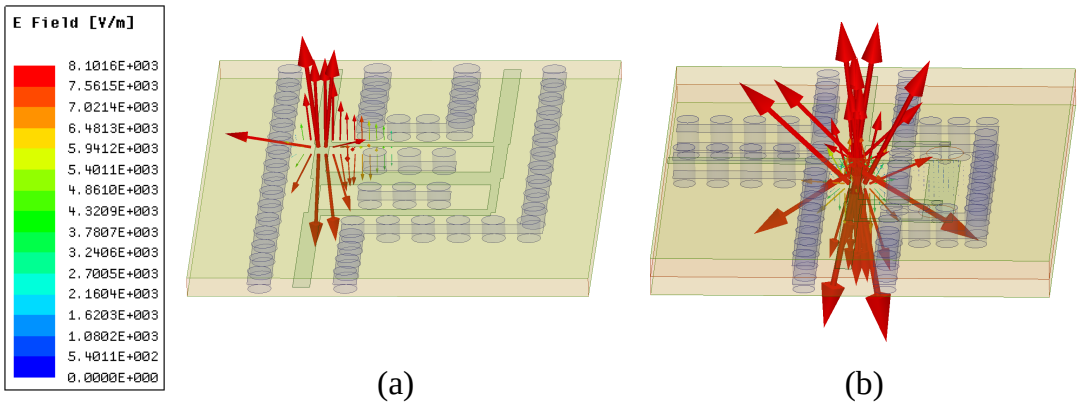

Figure 4.11 : E-field vector plot at 22 GHz for a) Planar SICL balun b) Folded SICL balun.

covering entire K-band. The folded balun occupies only 54.3% lateral area as compared to the planar wide-band SICL balun with a footprint of $0.76\lambda_g \times 0.44\lambda_g \times 0.1\lambda_g$. The folded balun works in 18 GHz to 26.6 GHz frequency range with a simulated 18 dB return loss, $\pm 1^\circ$ phase imbalance and ± 0.2 dB amplitude imbalance. Furthermore, the folded balun exhibits a fractional bandwidth of 37.27%. The folded wideband balun has smaller size for about the same bandwidth as planar SICL balun and this technique of designing an SICL balun resolves the problem of large size when extra stages of balun need to be cascaded for more bandwidth at the cost of increased fabrication complexity. SICL is a two conductor transmission line. The lateral metallic vias along with bottom and top ground plane form outer conductor, whereas the metallic strip sandwiched between the substrate makes the inner conductor of this planar dielectric filled coaxial line. The coaxial like radially outward directed E-field vector and concentric H-field in SICL transmission line are confirmed using Ansys HFSS and their field distribution has been shown in Fig. 1.5. In Fig. 4.11, the vector E-field for the planar and folded SICL based balun is presented. The radially outward vector E-field demonstrated in both the proposed SICL based wideband baluns prove that SICL is indeed the planar form of traditional coaxial line.

4.2 A SUBSTRATE INTEGRATED COAXIAL LINE DUAL-BAND BALUN FOR 5G APPLICATIONS

The advent of 5G communication has pushed for new design specification to be met for the overall system design. The FR-1 and FR-2 band of 5G communication covers the two important bands in microwave and millimeter-wave region [120]. In the following work the design of a dual-band substrate integrated coaxial line (SICL) balun operating at 6 GHz and 28 GHz for 5G application is proposed. This balun is realized using open-ended coaxial stubs with shielding as shown in Fig. 4.12. The performance of the dual-band SICL configuration is analyzed and range of realizable frequency ratios is determined from the analytically derived equations. The designed SICL based balun demonstrates low amplitude and phase imbalance in both the desired bands with good inter-band suppression making it worthy for practical applications. Proposed compact balun covers only $0.43\lambda_g \times 0.68\lambda_g$ circuit area.

4.2.1 Modeling of a Dual-Band Substrate Integrated Coaxial Line

The design of the proposed dual-band SICL based balun starts with modeling of a dual-band transmission line. The SICL based dual-band transmission line is composed of two series transmission line (Z_1, θ_1) with an open-ended coaxial stub (Z_2, θ_2) connected at its center. The entire configuration is delimited by rows of metalized-vias on both sides. The diameter of

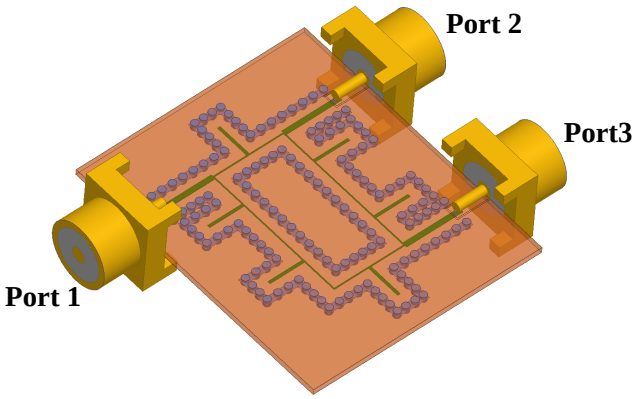

Figure 4.12 : Proposed SICL based dual-band balun for 5G applications.

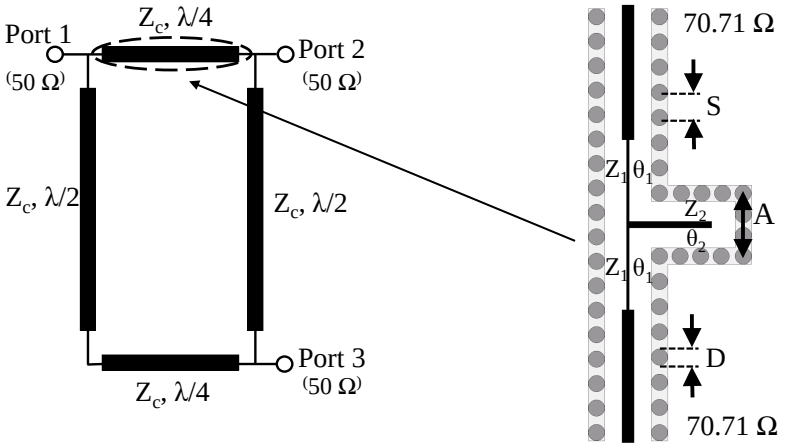

Figure 4.13 : Design of an SICL based dual-band transmission line model for a branch-line balun.

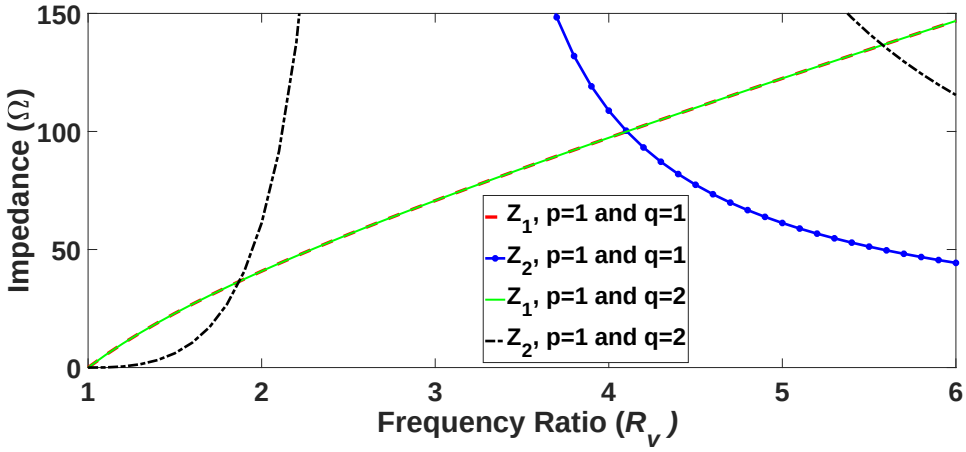

Figure 4.14 : Variation in Z_1 and Z_2 with respect to the frequency ratio (R_v).

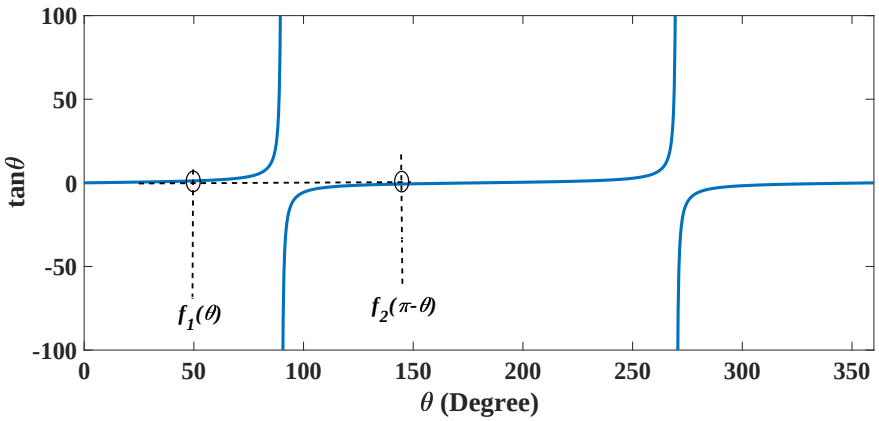

Figure 4.15 : Demonstration of dual-band characteristics for the proposed structure.

via is D, spacing between vias is S and distance between rows of vias is A as shown in Fig. 4.12. Proper choice of the parameters namely D, A and S enables the designer to ensure single-mode TEM propagation through the entire range of frequencies up to the next higher order-mode (TE_{10}). In the proposed configuration A = 2.5mm, S = 0.9mm and D = 0.6mm to ensure TEM mode propagation upto 48 GHz [51]. In order to have dual-band operating balun the proposed configuration should demonstrate $\pm 90^{\circ}$ phase shift at both design frequencies while maintaining a characteristic impedance of 70.71 Ω. This is ensured by equating the ABCD matrix of a conventional $\lambda/4$ transmission line of characteristic impedance Z_c [123] with the ABCD matrix of the configuration shown in Fig. 4.13. The derived equations are given as [124]:
ABCD Matrix of a conventional quarter-wavelength transmission line:

$$\begin{bmatrix} A & B \\ C & D \end{bmatrix}_{\lambda/4} = \begin{bmatrix} 0 & jZ_c \\ \frac{j}{Z_c} & 0 \end{bmatrix} \tag{4.3}$$

ABCD Matrix of the proposed configuration:

$$\begin{bmatrix} A & B \\ C & D \end{bmatrix} = M_1 M_2 M_1 \tag{4.4}$$

$$M_1 = \begin{bmatrix} \cos\theta_1 & jZ_1 \sin\theta_1 \\ \frac{j\sin\theta_1}{Z_1} & \cos\theta_1 \end{bmatrix} \tag{4.5a}$$

$$M_2 = \begin{bmatrix} 1 & 0 \\ \frac{j\tan\theta_2}{Z_2} & 1 \end{bmatrix} \tag{4.5b}$$

$$\begin{bmatrix} A & B \\ C & D \end{bmatrix} = \begin{bmatrix} \cos 2\theta_1 - \frac{Z_1}{2Z_2}\sin 2\theta_1 \tan\theta_2 & j2Z_1 \sin 2\theta_1 - \frac{jZ_1^2 \sin^2\theta_1}{\cot\theta_2} \\ jZ_1{}^2\left(\frac{\sin 2\theta_1}{Z_1} + \frac{\sin^2\theta_1 \tan\theta_2}{Z_2}\right) & \cos 2\theta_1 - \frac{Z_1}{2Z_2}\sin 2\theta_1 \tan\theta_2 \end{bmatrix} \tag{4.6}$$

Equating the ABCD matrix of a conventional $\lambda/4$ transmission line of characteristic impedance Z_c with the ABCD matrix of the configuration proposed SICL dual-band transmission line, the unknown characteristic impedances are determined as

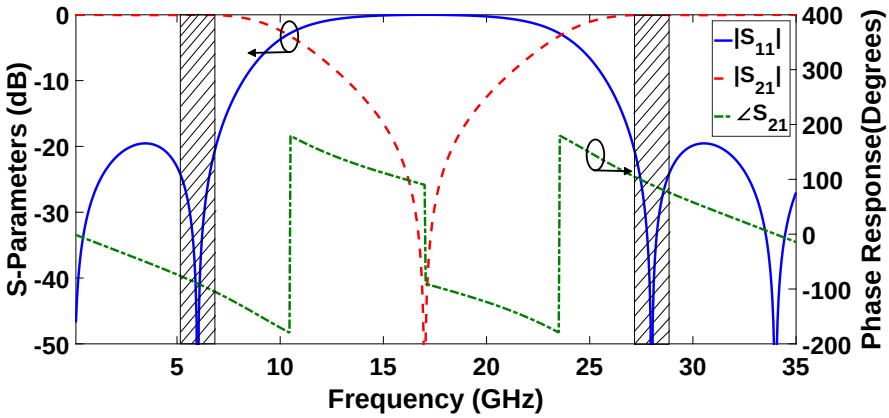

Figure 4.16 : Circuit simulated S-Parameters and phase response of the SICL based dual-band transmission line.

$$Z_1 = Z_c \cot(\theta_1) \tag{4.7}$$

$$Z_2 = \frac{Z_1 tan(2\theta_1)\tan(\theta_2)}{2} \tag{4.8}$$

In order to ensure $\pm 90^\circ$ phase shift at both design frequencies f_1 and f_2, the electrical length of the dual-band transmission line is chosen as

$$\theta_1 = t f_1 \tag{4.9}$$

$$\pi - \theta_1 = t f_2 \tag{4.10}$$

Solving (4.9) and (4.10)

$$\theta_1 = \frac{p\pi}{1+R_v}; \theta_2 = \frac{q\pi}{1+R_v} \tag{4.11}$$

R_v is the ratio of two design frequencies f_2/f_1. The variation in impedance Z_1 and Z_2 for different R_v derived using (4.7), (4.8) and (4.11) is depicted in Fig. 4.14. It is to be noted that by

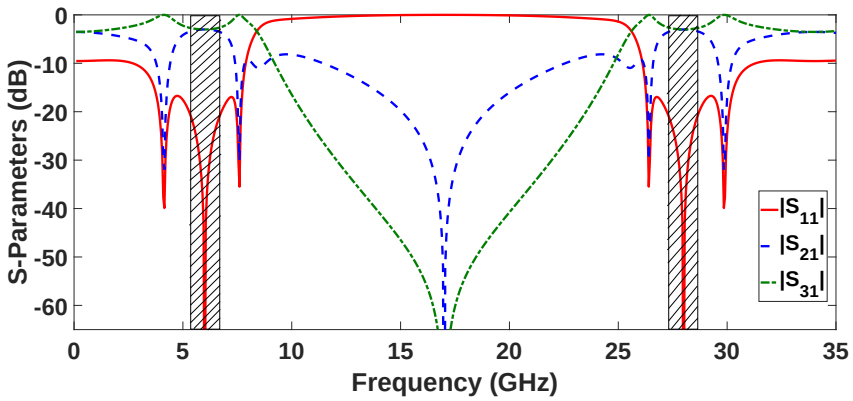

Figure 4.17 : Circuit-simulated S-parameters of the proposed dual-band balun.

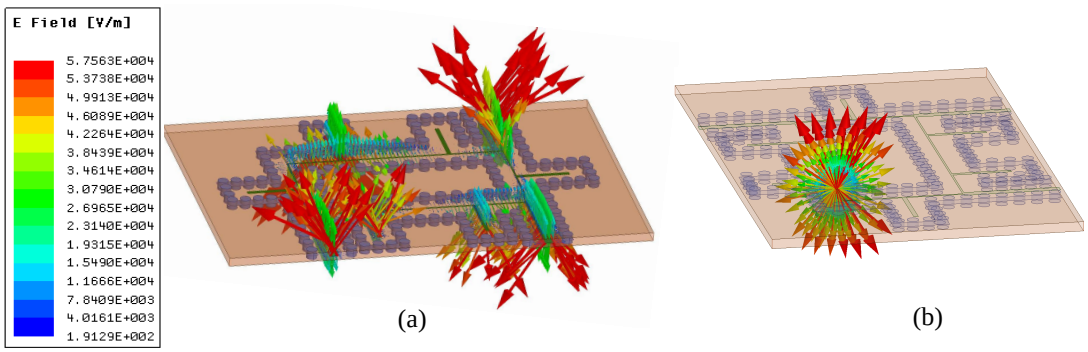

Figure 4.18 : E-field vector plot at 28 GHz demonstrating a) Balanced signals at output ports 2 & 3 b) Radially outward directed E-field inside SICL.

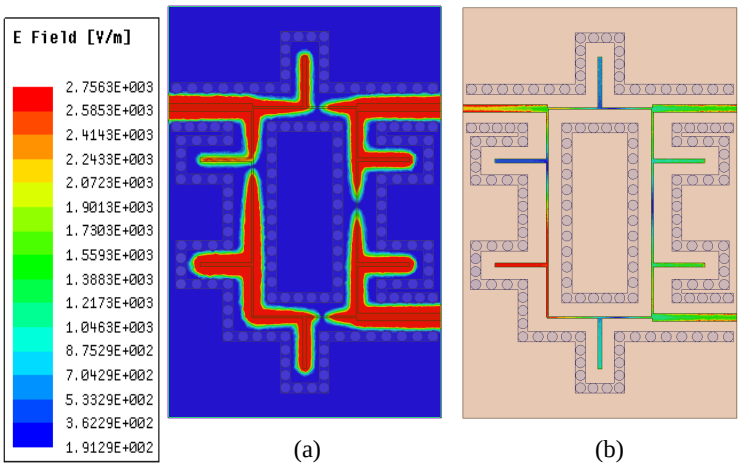

Figure 4.19 : Magnitude of E-field at 28 GHz a) On the top ground plane b) Inner conducting strip of SICL based dual-band balun.

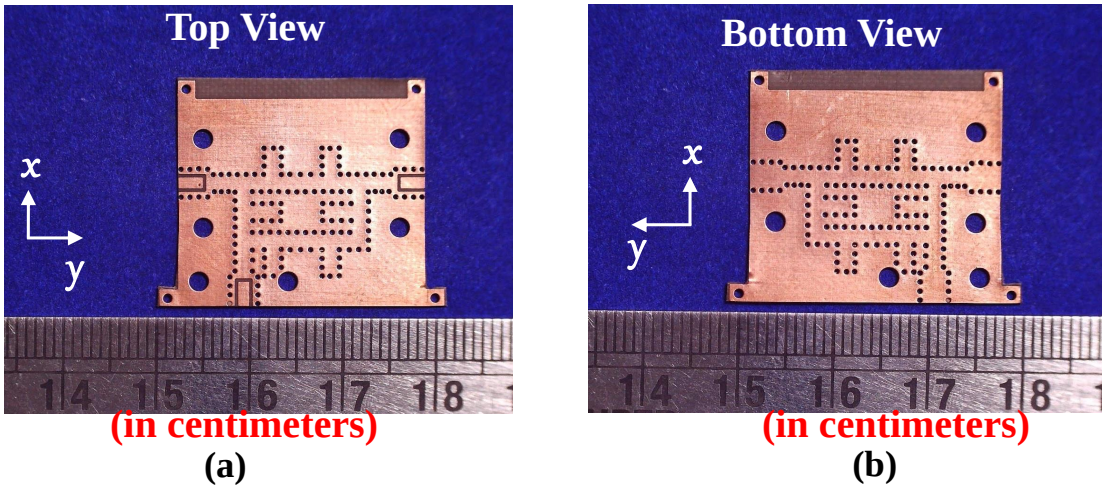

Figure 4.20 : Photograph of the fabricated compact dual-band SICL balun for 5G applications

changing p and q, required value of R_v can be realized within the fabrication limit. The span of realizable frequency ratio is from 3.7 to 6 considering Z_1 and Z_2 in the range of 20 Ω to 150 Ω.

From the design curve in Fig. 4.14 the unknown impedances are given as Z_1 = 114.2 Ω and Z_2 = 71.0 Ω for the required frequency ratio (R_v). The electrical length of the transmission line are chosen such that they demonstrate the same electrical length at both frequencies as shown in Fig 4.15. The total electrical length of the series transmission line is 63.52° and open-ended coaxial stub is 31.76° by choosing p = 1 and q = 1 in (4.11). The required characteristic impedance is realized by selecting the appropriate width of inner conducting strip and outer conductor by using the equation (2.9). The width of SICL inner conductor corresponding to impedances Z_1 and Z_2 are 0.1 mm and 0.24 mm respectively. In Fig. 4.16, the S-parameters and phase response of the configuration proposed is shown. It is observed that the phase of the proposed SICL based dual-band line is ±90° at both 6 GHz and 28 GHz with good impedance matching in both bands indicating the dual-band transmission line offers a characteristic impedance of 70.71 Ω at desired frequencies simultaneously. In Fig. 4.17 the circuit simulation of proposed dual-band balun

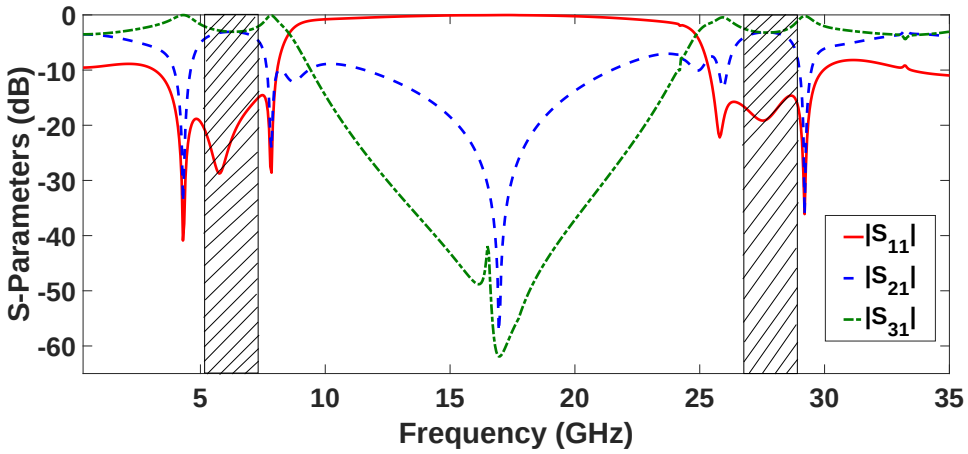

Figure 4.21 : Full-wave simulated S-Parameters of the proposed dual-band balun.

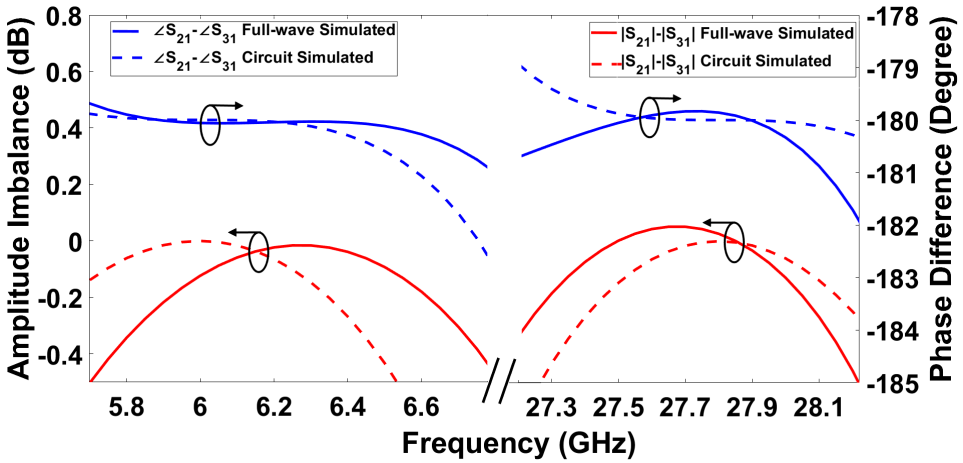

Figure 4.22 : Full-wave and circuit simulated magnitude imbalance and phase difference.

performed using Keysight's Advanced Design System (ADS) indicates good impedance matching with low amplitude and phase imbalance in both bands.

4.2.2 Design of Dual-band SICL Based balun

The proposed SICL dual-band section is used to replace all the conventional $\lambda/4$ arms of the commonly used branch-line balun as shown in Fig. 4.13. Two sheets of low loss Taconic TLY-5 (ε_r = 2.2, δ = 0.0009) substrate, each of thickness 0.254 mm bonded using Taconic FR-28 prepeg (ε_r = 2.74, tanδ = 0.0014) is considered. SICL to Grounded-coplanar waveguide transition (GCPW) is used to facilitate testing of the proposed dual-band balun using a K-connector as shown in Fig. 4.12. The transition is realized by connecting the conducting middle strip to the disconnected top ground plane using a metallic via. Due to the use of thin substrate very minor reactive component is contributed by this via at high frequencies and superior performance is achieved. The transformation of an unbalanced signal to a balanced form is observed from the out of phase signals present at the output ports as seen from the radially outward E-field vector plot at 28 GHz in Fig. 4.18(a). SICL is a two conductor transmission line. The lateral metallic vias along with bottom and top ground plane form outer conductor, whereas the metallic

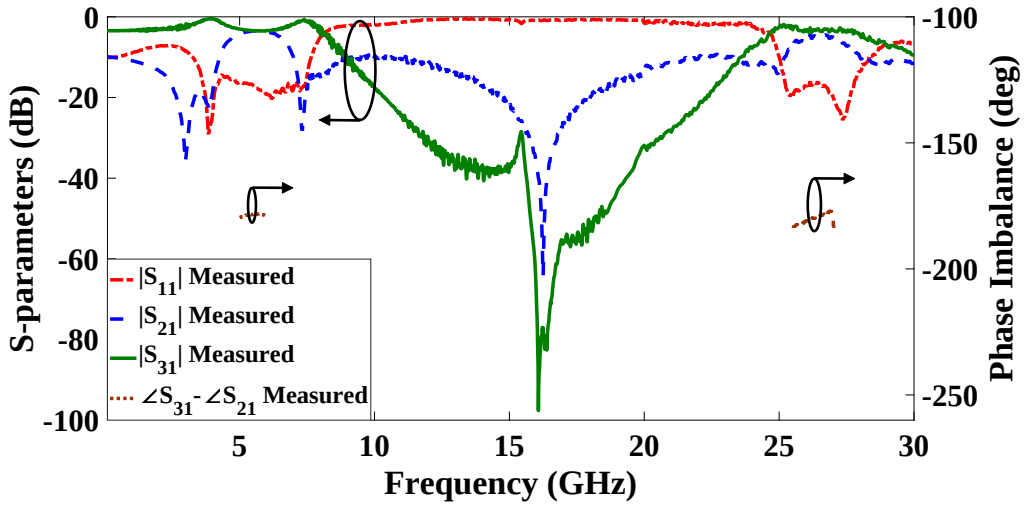

Figure 4.23 : Measured S-parameters and phase difference of the fabricated SICL based dual-band balun.

Table 4.2 : Full-wave simulated & measured specifications of the proposed dual-band SICL based balun

	Simulated		Measured	
	Band I	Band II	Band I	Band II
Dual-Band:	5.7GHz to 6.8GHz	27.12GHz to 28.25GHz	5.1GHz to 6.3GHz	26.5GHz to 27GHz
Fractional Bandwidth	17.6%	3.97%	19.13%	1.87%
Size:	$0.43\lambda_g \times 0.68\lambda_g$		$0.43\lambda_g \times 0.68\lambda_g$	
Return Loss	−19.3 dB	−19.5 dB	17.95	15.93
Magnitude imbalance	±0.5 dB	±0.5 dB	±1 dB	±1.5 dB
Phase imbalance	±2	±1.8°	±2°	±2.8°

strip sandwiched between the substrate makes the inner conductor of this planar dielectric filled coaxial line. The coaxial like radially outward directed E-field vector and concentric H-field in SICL transmission line are confirmed using Ansys HFSS and their field distribution has been shown in Fig. 1.5. The certainty of the proposed SICL based dual-band balun being the printed form of traditional coaxial line is verified by observing the radially outward directed E-field vector as shown in Fig. 4.18(b). In Fig. 4.19(a) magnitude of electric field distribution in the top ground plane at 28 GHz is presented. It is observed that the presence of vias mitigate the leakage of electromagnetic wave from the component to affect the neighboring circuits, thereby demonstrating robust electromagnetic compatibility. Equal-power division with good impedance matching between the output and input ports is proved by verifying the magnitude of electric field distribution through the inner conducting strip as portrayed in Fig. 4.19(b).

4.2.3 Results and Discussion

The proposed SICL based dual-band balun is fabricated with standard mulitlayer PCB fabrication technology, using two Taconic TLY-5A(ε_r = 2.2, tanδ = 0.0009) substrate, each of thickness 0.508 mm is bonded using Taconic FR-28 prepreg (ε_r = 2.74, tanδ = 0.0014) of 4 mil thickness. The photograph of the fabricated SICL based dual-band balun is shown in Fig. 4.20. The

performance of the proposed dual-band SICL based balun is verified through full-wave simulated S-parameters determined by Ansoft HFSS as well as measurement of fabricated prototype using Agilent N5234A (10 MHz to 43.5GHz) vector network analyzer. The full-wave simulated S-parameters of the designed balun is shown in Fig. 4.21. The full-wave simulated results good impedance matching and out of phase operation in the two desired bands as shown in Fig. 4.22. The specification of the proposed dual-band balun is listed in Table 4.2. The measured impedance matching is better than 15 dB both predicted frequency bands of 6 GHz and 28 GHz with good inter-band suppression of more than 28 dB as shown in Fig 4.23. The measured results indicate the frequency range 5.1 GHz to 6.3 GHz and 26.5 GHz to 27 GHz displays a magnitude imbalance better than $|S_{21}|$ - $|S_{31}|$ = $\pm$ 1.5 dB and phase imbalance better than $\angle S_{21}$ - $\angle S_{31}$ = $\pm$ 2.8°. The discrepancy between simulated and measured results, especially the shift in frequency at the second band is attributed to the fabrication tolerance in manufacturing and minor air gaps during the bonding of the multilayer PCB. The SICL based dual-band balun presented here occupies a total surface are of 15.7 mm $\times$ 21.46 mm or equivalently $0.43\lambda_g \times 0.68\lambda_g$, where λ_g is guided wavelength at 6 GHz . It is to be noted that compact size can be achieved by folding the open-ended coaxial stubs inside the unused area of the dual-band balun.

4.3 COMPACT SUBSTRATE INTEGRATED COAXIAL LINE QUADRATURE HYBRID WITH HARMONIC REJECTION

Quadrature hybrid/ branch line coupler (BLC) serves multiple purposes in a modern communication system. It is used as a quadrature splitter in IQ modulator, employed in butler matrix for steering the beam of antenna arrays an in double balanced mixer diode to suppress local oscillator (LO) signal at RF port. Furthermore, the 90° out-phase signals provided by branch line couplers are widely used to develop circularly polarized antennas for cubesats & in linear to circular polarization converters. This widespread utilization of branch-line couplers motivates to investigate design in compact form-factor with enhanced functionalities.

4.3.1 Modeling of a compact SICL quadrature hybrid with controllable harmonic rejection

The three-dimensional stack up of the proposed SICL based quadrature hybrid is presented in Fig. 4.24. It is devised using open-ended coaxial stubs at all four ports of the branch-line structure with delimiting metallic vias running along the inner conductor. The equivalent transmission line model of the proposed BLC is shown as in Fig. 4.25. It comprises of vertical and horizontal arms of characteristic impedance Z_a and Z_b, respectively with equal electrical length θ_1. The open-ended stubs have a characteristic impedance Z_c with electrical length θ_2. The simplified circuit after even-odd analysis is shown in Fig. 4.26 and the input admittance computed by looking into port 1 is given as 4.12(a) - 4.12(d),

$$Y_{ee} = j\frac{\tan\left(\theta_1/2\right)}{Z_a} + j\frac{\tan\left(\theta_1/2\right)}{Z_b} + j\frac{\tan\theta_2}{Z_c} \tag{4.12a}$$

$$Y_{eo} = j\frac{\tan\left(\theta_1/2\right)}{Z_a} - j\frac{cot\left(\theta_1/2\right)}{Z_b} + j\frac{\tan\theta_2}{Z_c} \tag{4.12b}$$

$$Y_{oe} = -j\frac{\cot\left(\theta_1/2\right)}{Z_a} + j\frac{tan\left(\theta_1/2\right)}{Z_b} + j\frac{\tan\theta_2}{Z_c} \tag{4.12c}$$

$$Y_{oo} = -j\frac{cot\left(\theta_1/2\right)}{Z_a} - j\frac{cot\left(\theta_1/2\right)}{Z_b} + j\frac{\tan\theta_2}{Z_c} \tag{4.12d}$$

The unknown impedances of the proposed branch-line coupler are calculated by equating

the even and odd mode admittance of the proposed hybrid with that of a conventional branch line coupler [125] designed using $\lambda_g/4$ transmission lines with characteristic impedance Z_o = 50 Ω. Z_a, Z_b and Z_c are derived as:

$$Z_a = \frac{Z_o}{2}\left(\tan\left(\theta_1/2\right) + cot\left(\theta_1/2\right)\right) \tag{4.13a}$$

$$Z_b = \frac{Z_o}{2\sqrt{2}}\left(\tan\left(\theta_1/2\right) + cot\left(\theta_1/2\right)\right) \tag{4.13b}$$

$$Z_c = \frac{\tan\theta_2}{Q_1} \tag{4.13c}$$

where Q_1 is given as,

$$Q_1 = \frac{1+\sqrt{2}}{Z_o}\left(1 - \frac{2\tan\left(\theta_1/2\right)}{\tan\left(\theta_1/2\right) + cot\left(\theta_1/2\right)}\right)$$

To design a compact quadrature hybrid, θ_1 is kept less than 90°. Here, θ_1 is chosen as 72° to achieve 20% size reduction as compared to the traditional $\lambda_g/4$ line. The length of coaxial open stub θ_2 is chosen such that it generates a transmission zero at the frequency they are quarter-wavelength long. In order to achieve wide stop-band response a transmission zero at $2.5f_o$ is generated by selecting θ_2 = 36°. Further solving 4.13(a) - 4.13(c), graphically, a design curve as shown in Fig. 4.27(a) is obtained for Z_a , Z_b, and Z_c as a function of θ_1 by keeping θ_2 as constant. The circuit

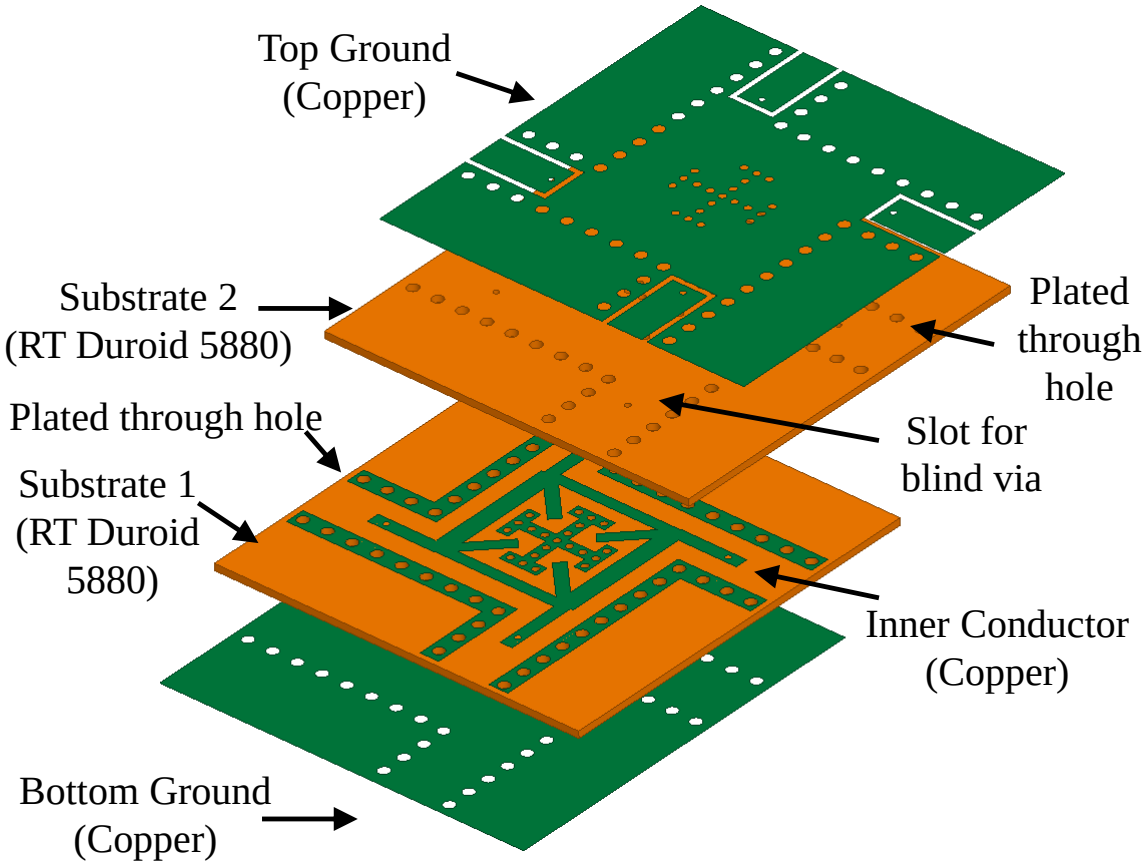

Figure 4.24 : Three dimensional view of the proposed SICL quadrature hybrid.

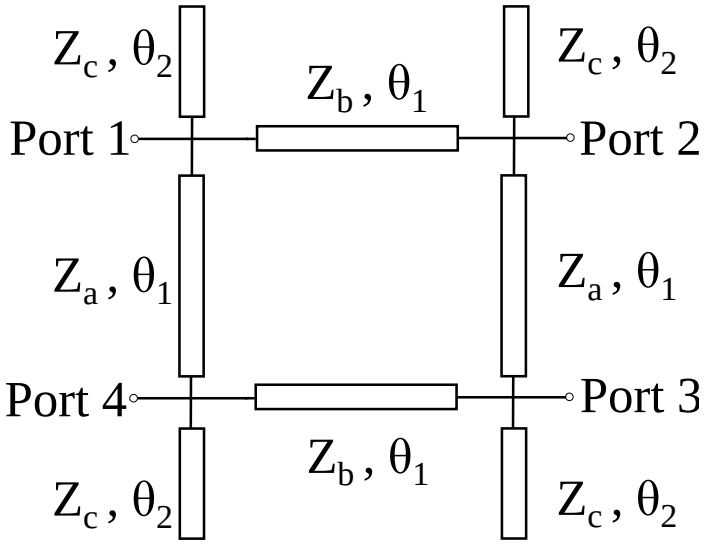

Figure 4.25 : Equivalent transmission line model of the proposed SICL based compact quadrature hybrid

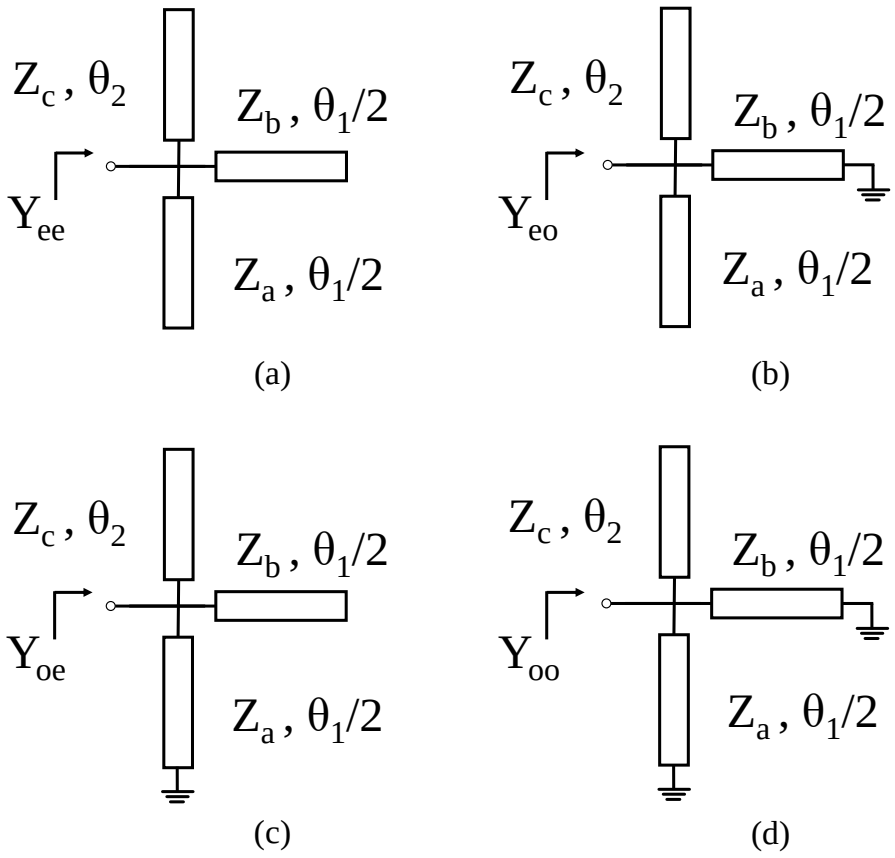

Figure 4.26 : Second-order even-odd mode analysis of the proposed harmonic suppressed BLC (a) Even-even mode (b) Odd-even mode (c) Even-odd mode (d) Odd-odd mode

simulated results plotted using ADS is depicted in Fig. 4.27(b). The controllability in harmonic

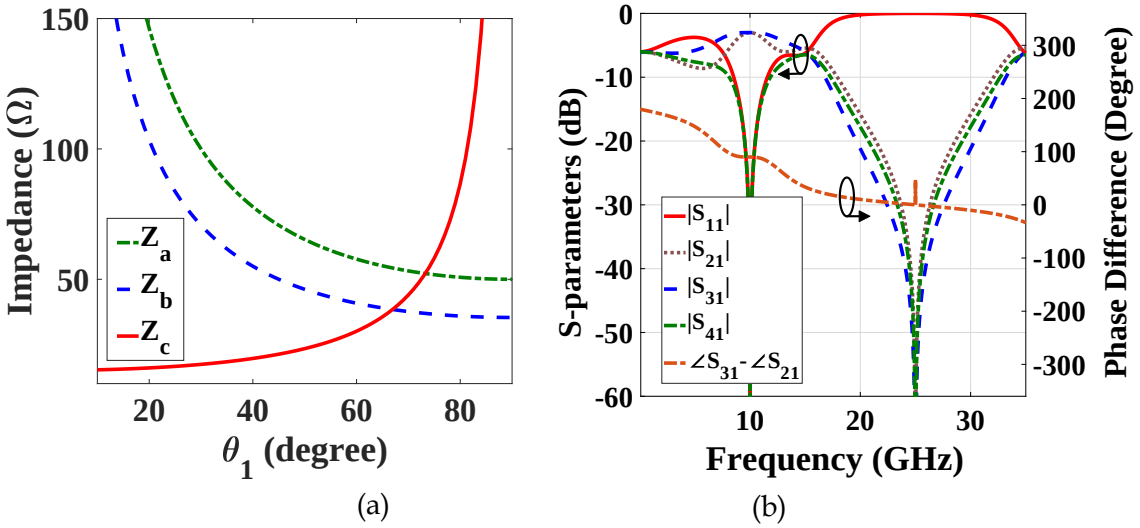

Figure 4.27 : (a) Design curve as a function of θ_1 for fixed $\theta_2 = 36^\circ$ to calculate the unknown impedances (b) Circuit simulated S-parameters and phase difference with parameters Z_a = 52.57 Ω, Z_b = 37.17 Ω, Z_c = 48.69 Ω, $\theta_1 = 72^\circ$ and $\theta_2 = 36^\circ$.

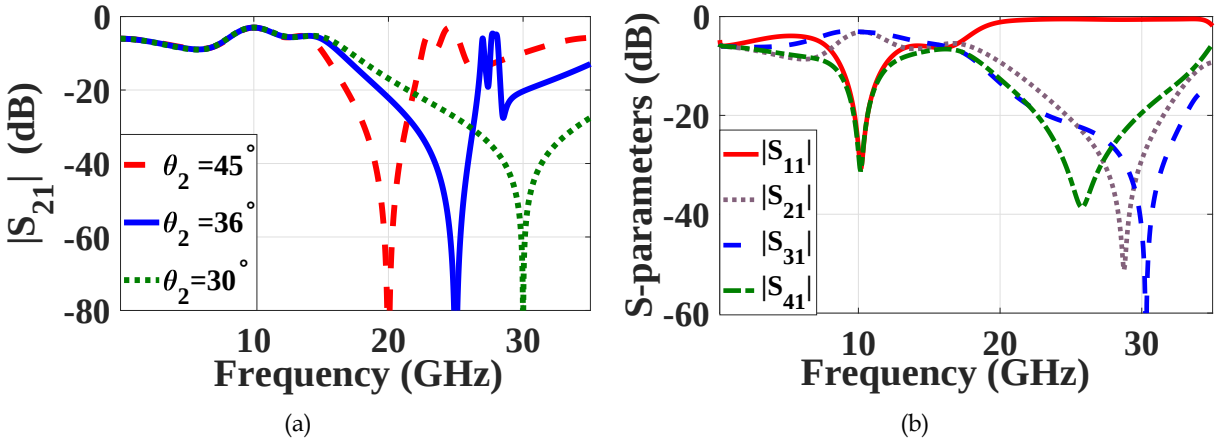

Figure 4.28 : Study on proposed SICL based quarature hybrid (a) variation in stop-band response with change in θ_2 for fixed $\theta_1 = 60^\circ$ (b) Full-wave simulated S-parameters

rejection has been demonstrated in Fig. 4.28 (a) by varying the length of coaxial open stub θ_2 for fixed $\theta_1 = 60^\circ$. The full-wave simulated S-parameters generated using Ansys HFSS is shown in Fig:Variation in stop-band response with change HBLC (b).

4.3.2 Results And Discussion

The proposed BLC is fabricated using a pair of Taconic TLY-5A (ε_r = 2.2, tanδ = 0.0009) substrate each of thickness 0.254 mm. The theoretical analysis is validated by measuring the S-parameters of the fabricated coupler with Agilent's E5071C network analyzer of frequency range 300 kHz to 20 GHz. The geometrical layout of the proposed configuration with dimensions is presented in Fig. 4.29(a) and photograph of the fabricated prototype is shown in Fig. 4.29(b). A SICL to GCPW transition is realized using a blind via connecting the 50Ω SICL transmission line

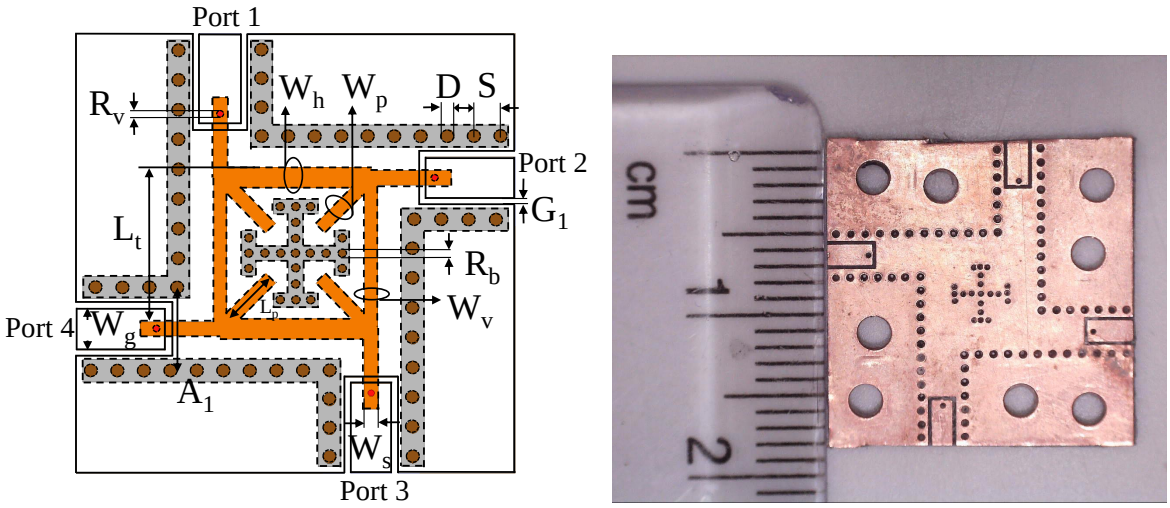

Figure 4.29 : Proposed compact harmonic suppressed SICL quadrature hybrid (a) Geometrical layout of the proposed SICL based quadrature hybrid with dimensions: A_1 = 2.1mm, D = 0.6mm, G_1 = 0.2mm, S = 0.9mm, R_b = 0.3mm, R_v = 0.2mm, L_t = 4.72mm, L_p = 2.23mm, W_h = 0.65mm , W_g = 1.3mm, W_p = 0.42mm, W_s = 0.45mm, and W_v = 0.4mm. (b) Photograph of the fabricated compact harmonic suppressed SICL quadrature hybrid.

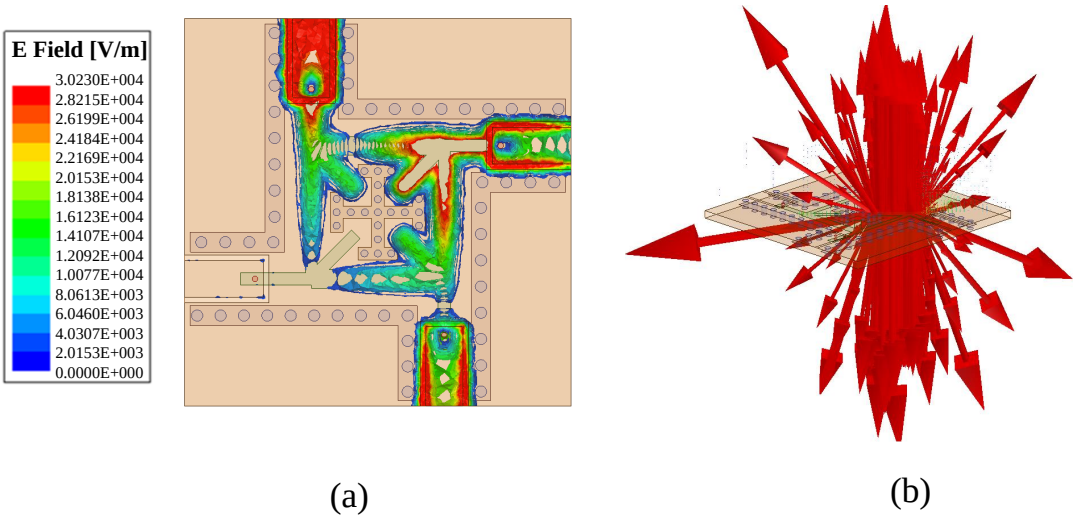

Figure 4.30 : Electric field distribution at 10 GHz (a) Magnitude of E-field demonstrating shielding between open-ended stubs b) E-field vector plot.

to GCPW transmission line located along with top ground plane of SICL. As we know, SICL is a two conductor transmission line form with lateral metallic vias along with bottom and top ground plane forming outer conductor and whereas the metallic strip sandwiched between the substrate makes the inner conductor of this planar dielectric filled coaxial line. The coaxial like radially outward directed E-field vector and concentric H-field in SICL transmission line are confirmed using Ansys HFSS and their field distribution has been shown in Fig. 1.5. From the magnitude of E-field shown in Fig. 4.30(a) the motivation behind arrangement of vias in the inner section to

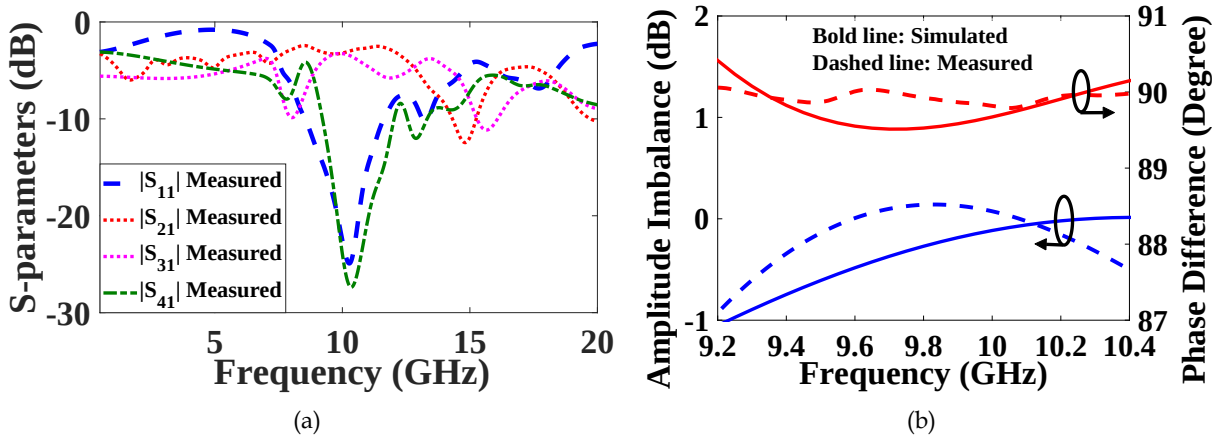

Figure 4.31 : Comparison between measured and full-wave simulated (a) S-parameters (b) magnitude imbalance and phase difference of the proposed SICL based BLC

provide the necessary shielding between the open-ended coaxial stubs can be perceived. Further, the radially outward vector electric field in Fig. 4.30(b) exhibits field distribution similar to that of traditional coaxial line thereby confirming SICL to be coaxial line in planar form. A measured return loss and isolation better than 20 dB with equal power division at output ports is observed at 10 GHz in Fig. 4.31 (a) with at least 15 dB harmonic rejection till 31.8 GHz is verified through full-wave simulation in HFSS. Though the proposed quadrature hybrid demonstrates potential to work up to 35 GHz, measured results till 20 GHz has been reported in this work due to limitation in measurement setup. In Fig. 4.31 (b), magnitude imbalance less than $|S_{21}|$ - $|S_{31}|$ = $\pm$1 dB and phase imbalance better than $\angle S_{21}$ - $\angle S_{31}$ = $\pm 0.5^{\circ}$ in the frequency range of 9.2 GHz to 10.4 GHz is measured. The proposed SICL quadrature hybrid for X-band communication demonstrates a fractional bandwidth of 12.24%. The designed SICL quadrature hybrid occupies 6.87 mm $\times$ 6.87 or equivalently $0.33\lambda_g \times 0.33\lambda_g$ excluding the transition, where λ_g is guided wavelength at 10 GHz.

4.4 DESIGN OF A WIDEBAND BRANCH-LINE COUPLER FOR K_U-BAND

4.4.1 Theoretical analysis of a wideband branch line coupler

The schematic of a two-stage branch-line coupler is shown in Fig. 4.32. A 3-dB branch-line coupler comprising of four-ports offers equal power division with 90 $^{\circ}$ phase difference between its through and coupled arm. The [S]-matrix of this four-port network is given by (4.14):

$$[S] = \frac{-1}{\sqrt{2}} \begin{bmatrix} 0 & j & 1 & 0 \\ j & 0 & 0 & 1 \\ 1 & 0 & 0 & j \\ 0 & 1 & j & 0 \end{bmatrix} \tag{4.14}$$

All the arms of the proposed two-stage SICL based 3-dB branch line coupler are maintained at θ, where $\theta = 90^{\circ}$ at the design frequency 15 GHz with characteristic impedances as shown in Fig. 4.32. From the schematic it is observed the branch line coupler maintains high degree symmetry since any port can be used as the input port. To simplify the analysis, the circuit is decomposed to its constituent even and odd components as shown in Fig. 4.33. The input admittance calculated by looking into port 1 of the reduced equivalent circuits are given by equation (4.15).

$$Y_{ee} = \frac{j\tan\left(\theta/2\right)}{Z_b} + \frac{j}{Z_a}\frac{Z_a + 2Z_c\cot\left(\theta/2\right)\tan\theta}{2Z_c\cot\left(\theta/2\right) - Z_a\tan\theta} \tag{4.15a}$$

$$Y_{eo} = \frac{j\tan\left(\theta/2\right)}{Z_b} - \frac{j\cot\theta}{Z_a} \tag{4.15b}$$

$$Y_{oe} = -\frac{j\cot\left(\theta/2\right)}{Z_b} - \frac{j}{Z_a}\frac{Z_a - 2Z_c\tan\left(\theta/2\right)\tan\theta}{2Z_c\tan\left(\theta/2\right) + Z_a\tan\theta} \tag{4.15c}$$

$$Y_{oo} = -\frac{j\cot\left(\theta/2\right)}{Z_b} - \frac{j\cot\theta}{Z_a} \tag{4.15d}$$

The reflection coefficients of the reduced equivalent even/odd mode mode circuits are computed using (4.16).

$$\Gamma_{ee} = \frac{1 - Z_0 Y_{ee}}{1 + Z_0 Y_{ee}} \tag{4.16a}$$

$$\Gamma_{eo} = \frac{1 - Z_0 Y_{eo}}{1 + Z_0 Y_{eo}} \tag{4.16b}$$

$$\Gamma_{oe} = \frac{1 - Z_0 Y_{oe}}{1 + Z_0 Y_{oe}} \tag{4.16c}$$

$$\Gamma_{oo} = \frac{1 - Z_0 Y_{oo}}{1 + Z_0 Y_{oo}} \tag{4.16d}$$

Finally, the S-parameters of the proposed two-stage branch-line hybrid is derived using (4.16).

$$S_{11} = \frac{\Gamma_{ee} + \Gamma_{eo} + \Gamma_{oe} + \Gamma_{oo}}{4} \tag{4.17a}$$

$$S_{21} = \frac{\Gamma_{ee} - \Gamma_{eo} + \Gamma_{oe} - \Gamma_{oo}}{4} \tag{4.17b}$$

$$S_{31} = \frac{\Gamma_{ee} - \Gamma_{eo} - \Gamma_{oe} + \Gamma_{oo}}{4} \tag{4.17c}$$

$$S_{41} = \frac{\Gamma_{ee} + \Gamma_{eo} - \Gamma_{oe} - \Gamma_{oo}}{4} \tag{4.17d}$$

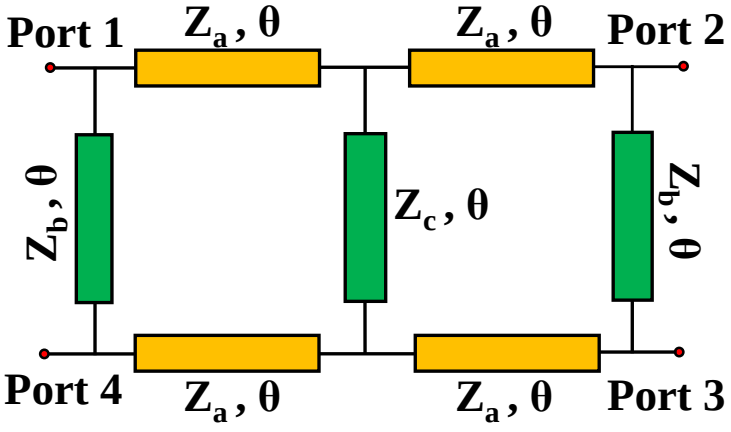

Figure 4.32 : Schematic of wideband two-stage branch line coupler.

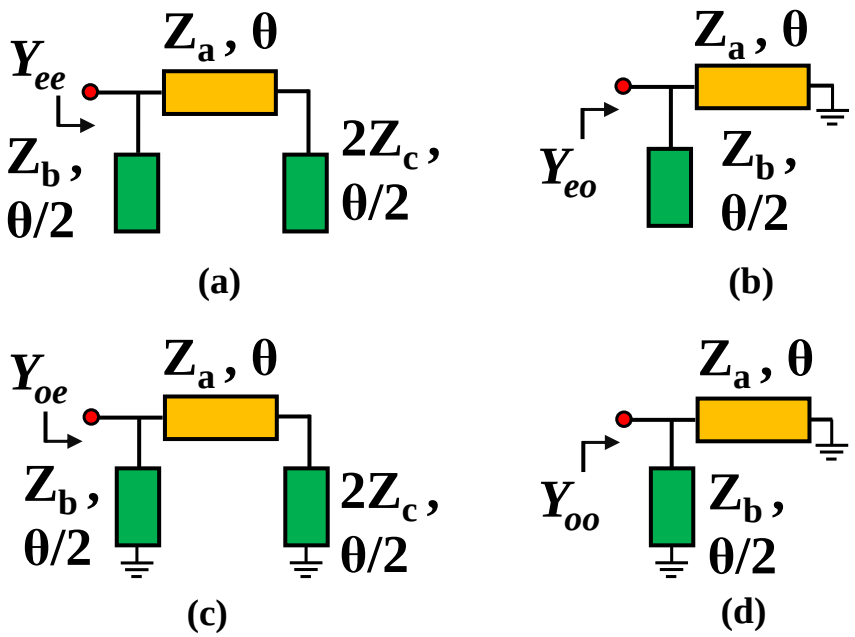

Figure 4.33 : Decomposition of two-stage branch line coupler into (a) Even-even (b) Even-odd (c) Odd-even (d) Odd-odd.

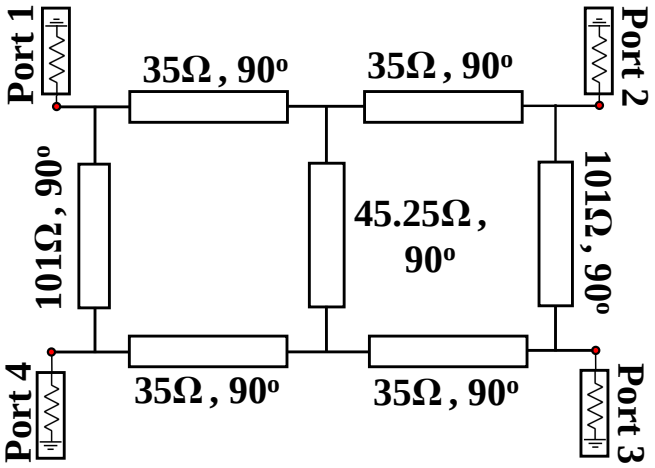

Figure 4.34 : Circuit simulation model of a two-stage branch line coupler.

To calculate the unknown characteristic impedances, S-parameters of proposed coupler in (4.17) are equated with the S-parameters of traditional 3-dB coupler in (4.14). The obtained transcendental equations are optimized to achieve amplitude imbalance less than 1 dB and phase imbalance less than 0.5°. The characteristic impedance of the line are chosen as Z_a = 35 Ω, Z_b = 101 Ω, and Z_c = 45.25 Ω. The working of proposed two-stage coupler is verified analytically by computing the S-parameters (4.17) using MATLAB and by simulating the circuit model of branch line coupler using ideal transmission lines in Keysight ADS software as shown in Fig. 4.34. In Fig. 4.35, the analytical and circuit simulated S-parameters are found to be in excellent agreement.

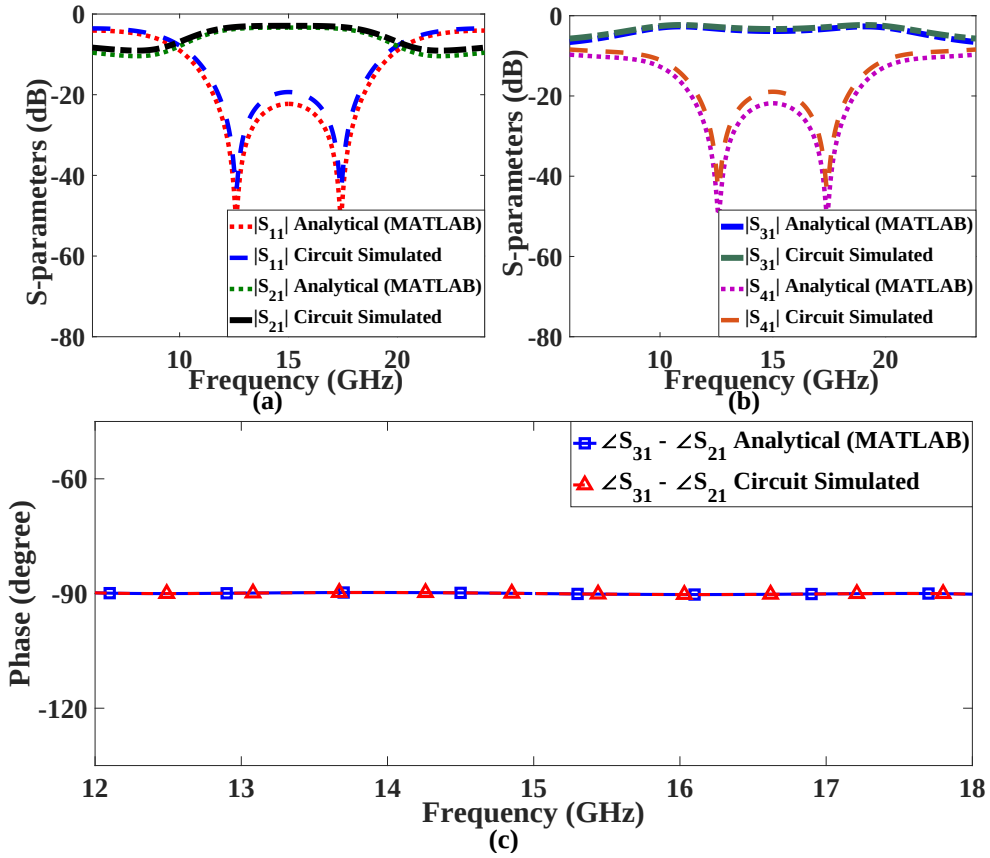

Figure 4.35 : Comparison between analytical and circuit simulated results of the proposed two-stage branch-line coupler (a) reflection coefficient and transmission coefficient (b) coupling coefficient and isolation (c) Phase difference between output ports

4.4.2 Synthesis of SICL based wideband branch line coupler

The geometrical layout of the proposed SICL based wideband branch line coupler is shown in Fig. 4.36. The proposed SICL based branch line coupler with metallized-vias along the inner and outer perimeter of the branch line coupler with top and bottom ground plane form the outer-conductor of this planar coaxial line. The diameter of via and pitch between vias are chosen carefully to avoid any wave-leakage from this shielded structure. Further, the distance between via rows (A_b) is selected such that single-mode TEM propagation is maintained throughout the band of operation [51]. The length of all arms are quarter-wavelength long at 15 GHz and characteristic impedance of each SICL arm is obtained by selecting the appropriate width of inner conducting strip and outer conductor by using the equation (2.9). The ports of the SICL based coupler have GCPW based transition at each feed line arranged orthogonal to each other to facilitate the mounting of super-SMA connectors.

4.4.3 Results and Discussion

The proposed planar SICL based wideband two-stage branch line coupler is implemented by enclosing the inner conducting strip between two Taconic TLY-5A (ε_r = 2.2, δ = 0.0009) substrates, each of thickness 0.254 mm bonded using Taconic FR-28 prepeg (ε_r = 2.74, tanδ = 0.0014). Since the inner conductor of SICL is not exposed, an SICL to GCPW transition is used for testing the prototype with a standard Super SMA mountable connector. The theoretical analysis is validated by measuring the S-parameters of the fabricated coupler with Agilent's E5071C network

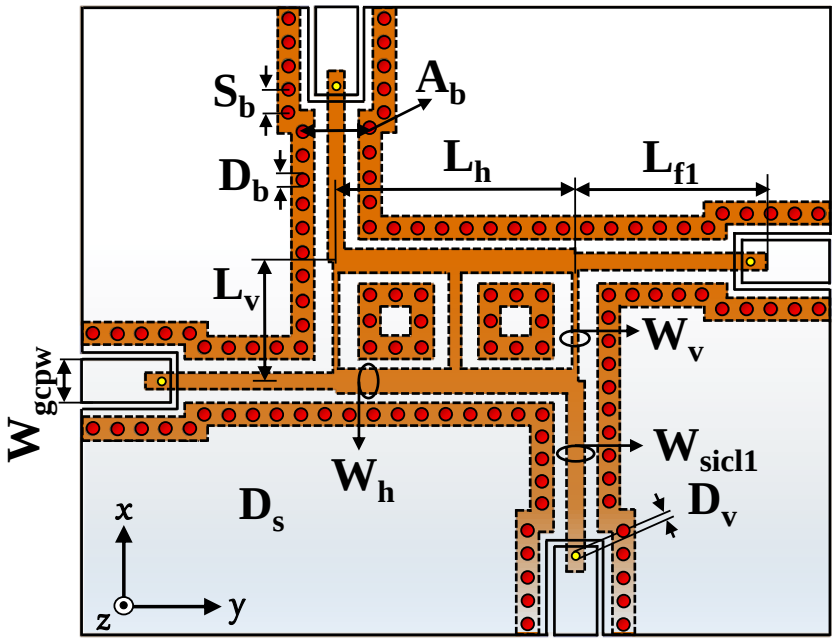

Figure 4.36 : Geometrical layout of the proposed wideband SICL two-stage branchline coupler with dimensions: A_b = 2.1mm, D_b = 0.4mm, D_v = 0.24mm, S_b = 0.74mm, L_{f1} = 6mm, L_h = 7.6mm, L_v = 3.51mm, W_h = 0.75mm, W_{gcpw} = 1.35mm, W_{sicl1} = 0.48mm, W_v = 0.15mm

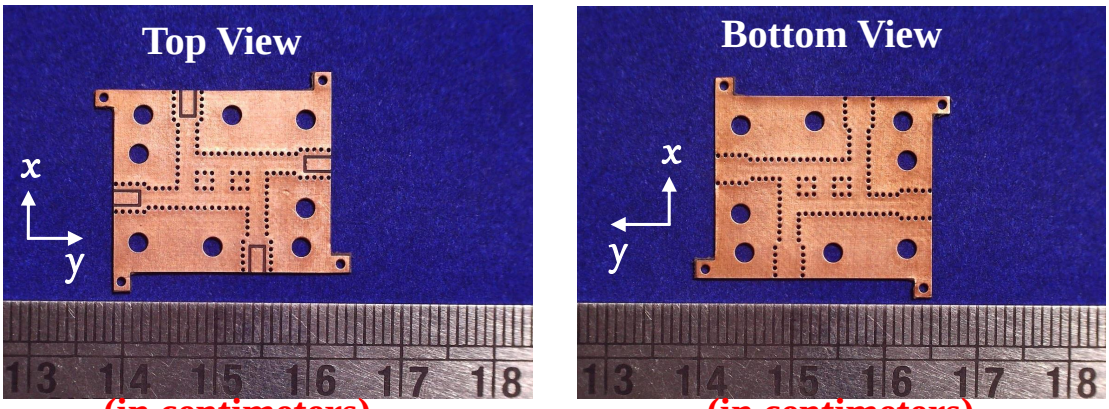

Figure 4.37 : Photograph of the fabricated two-stage wideband SICL based branch line coupler

analyzer of frequency range 300 kHz to 20 GHz. The photograph of the fabricated experimental prototype is shown in Fig. 4.37. A measured return loss and isolation better than 14 dB respectively, with amplitude imbalance less than ±1.5 dB at in the frequency band covering 12 GHz to 18 GHz as shown in Fig. 4.38. In Fig. 4.39, phase imbalance better than $\angle S_{21}$ - $\angle S_{31}$ = ±2° in the frequency range of 12 GHz to 18 GHz is validated through measurement from VNA. The proposed SICL based wideband branch-line coupler finds application in Ku-band communication and demonstrates a fractional bandwidth of 40% covers a lateral foot print 9.62 mm × 5.86 or equivalently $0.71\lambda_g \times 0.43\lambda_g$ excluding the transition, where λ_g is guided wavelength at 15 GHz.

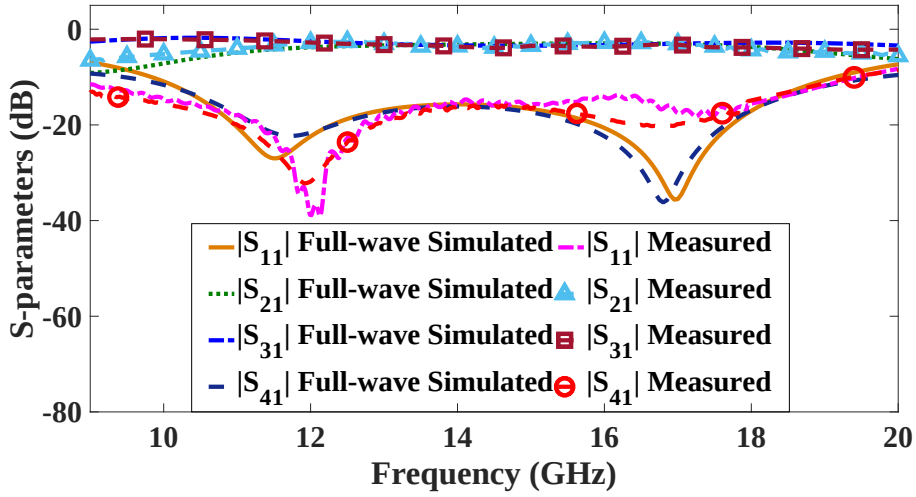

Figure 4.38 : Comparison between full-wave simulated and measured S-parameters of the proposed two-stage wideband SICL based branch line coupler.

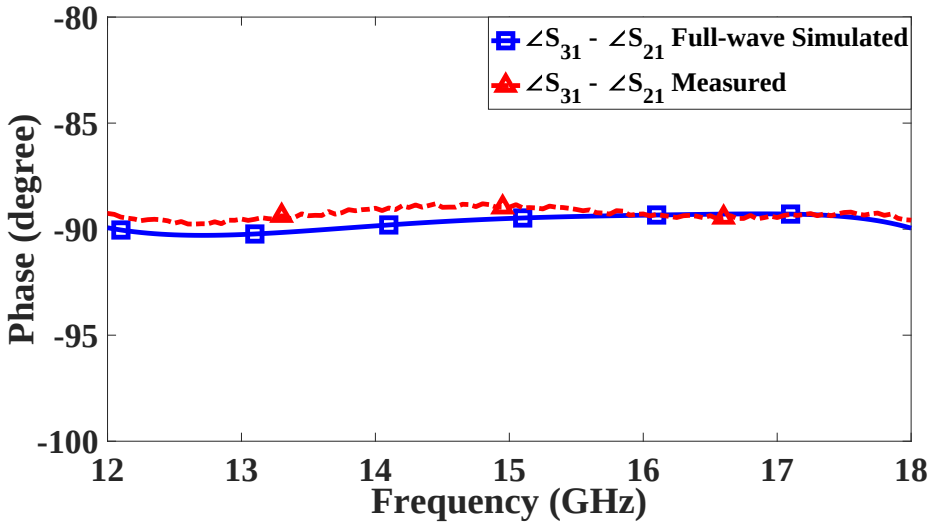

Figure 4.39 : Full-wave simulated and measured phase difference between output ports of the proposed two-stage SICL based branch line coupler.

4.5 DUAL-BROADBAND TWO-STAGE SUBSTRATE INTEGRATED COAXIAL LINE RAT-RACE COUPLER FOR X-BAND AND K-BAND WITH HARMONIC SUPPRESSION

So far in the previously proposed designs, single-band, dual-narrow band and wideband based three/four port networks have been explored. In the following work a dual-broadband substrate integrated coaxial line (SICL) based rat-race coupler functioning in *X* and *K*-band is proposed. A dual-band SICL transmission line is developed in this work using short-circuited planar coaxial stubs to replace the conventional quarter-wavelength transmission line. The operation of SICL based dual-band line is analyzed for various characteristic impedances and the range of realizable frequency ratios is determined analytically. The proposed SICL based rat-race coupler developed using dual-band transmission line is realized by standard PCB fabrication process and tested using a vector network analyzer. Owing to filtering response provided by

the short circuited coaxial stubs, the third-harmonic of the proposed coupler is suppressed and spurious rejection better than 22 dB is achieved up to 40 GHz.

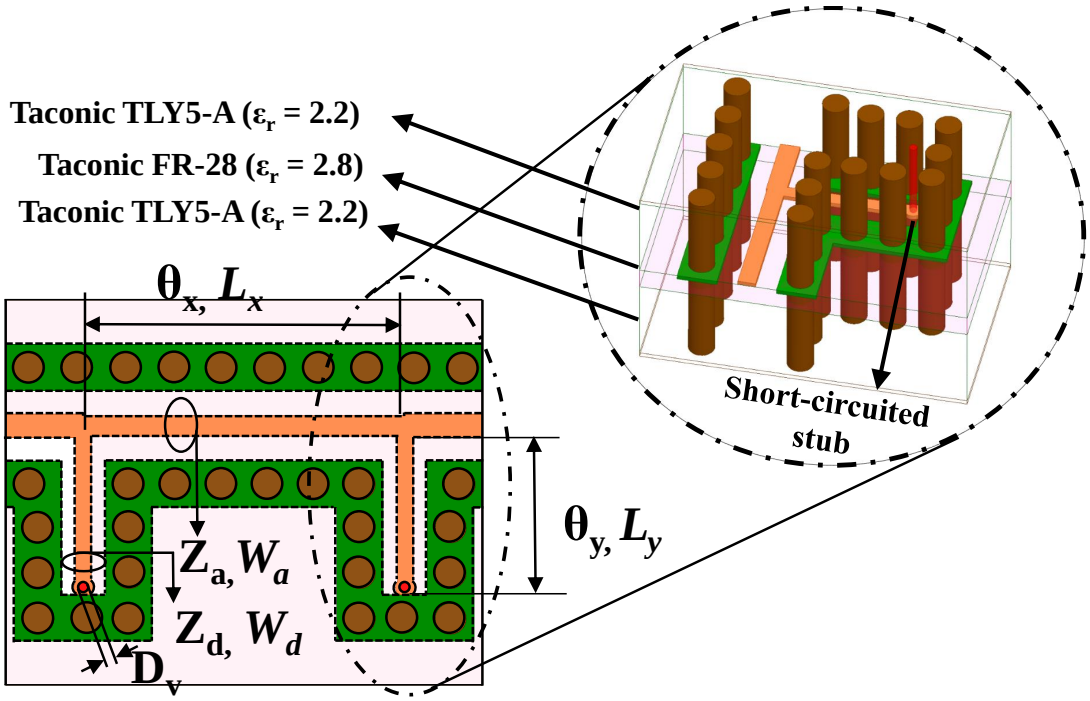

Figure 4.40 : Modeling of proposed substrate integrated coaxial technology based dual-band transmission line with dimensions: D_v = 0.2mm, L_x = 6.2mm, L_y = 3.256mm, W_a = 0.4mm, W_b = 0.3mm.

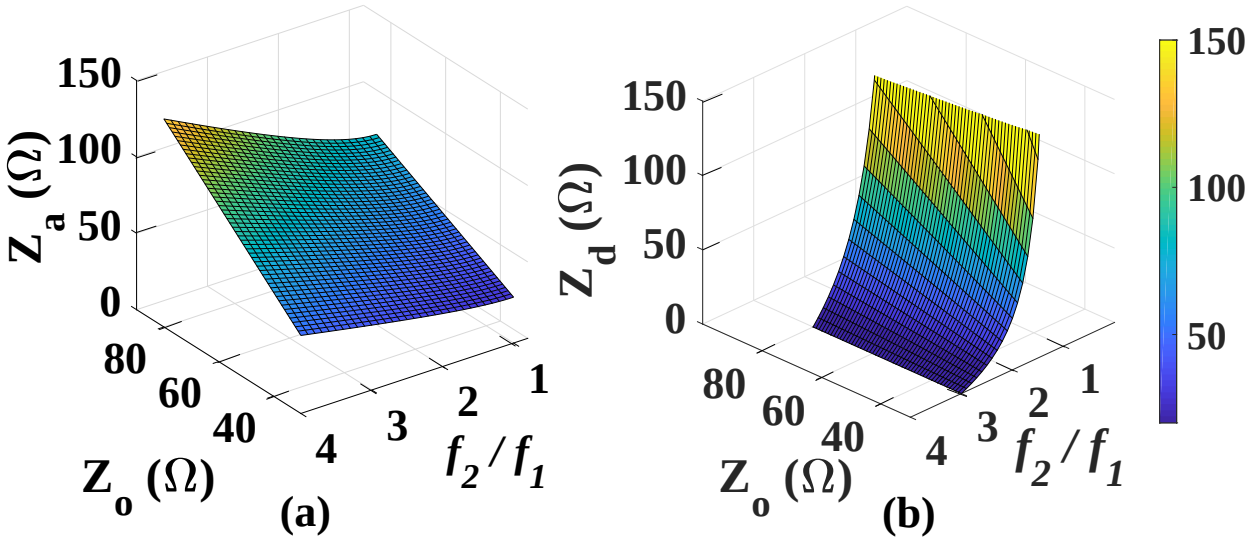

Figure 4.41 : Design curve to determine the realizable range of Z_a and Z_d of the proposed SICL based dual-band line by varying Z_o and frequency ratio (k).

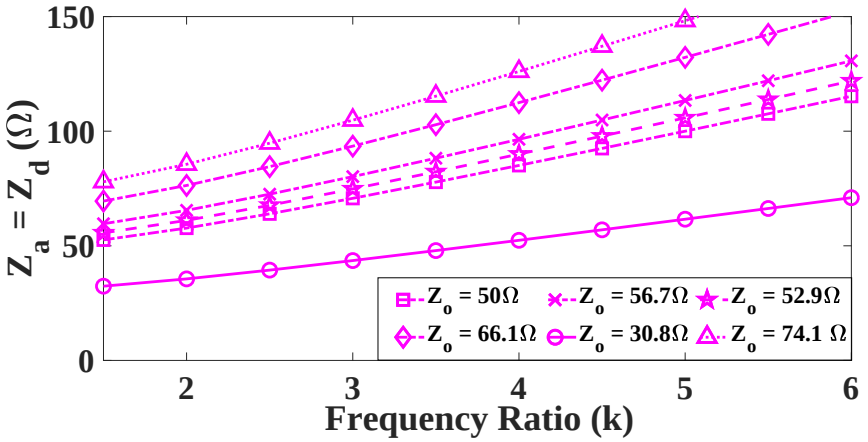

Figure 4.42 : Graphical solution of Z_a and Z_b as a function of frequency ratio (k) for case I: m = n = 1.

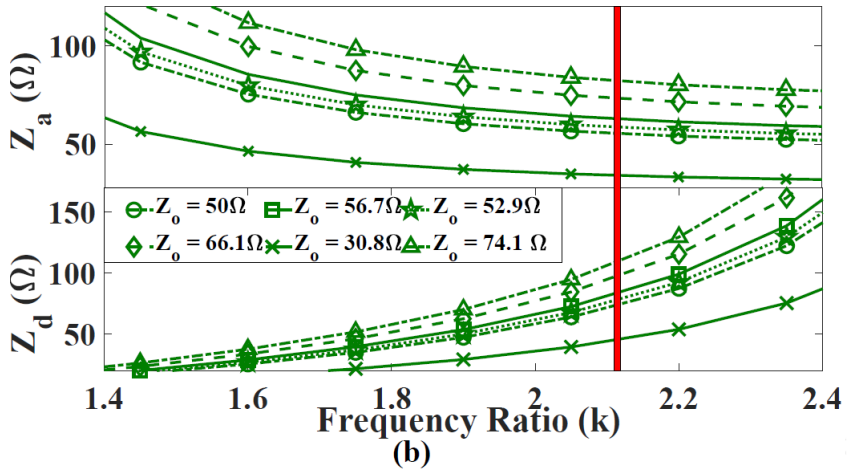

Figure 4.43 : Graphical solution of Z_a and Z_b as a function of frequency ratio (k) for case I: m = 2, n = 1.

4.5.1 Modeling of a dual-band transmission line featuring harmonic suppression

The physical layout and the layer-wise stack up of the proposed SICL based dual-band transmission line up is shown in Fig. 4.40. It is constructed using a series transmission line of characteristic impedance Z_a and electrical length θ_x with short-circuited planar coaxial stubs of characteristic impedance Z_b and electrical length θ_y tapped on both sides of the series transmission line. The proposed SICL based transmission line consists of a conducting strip sandwiched between two-dielectrics using a pre-preg layer. As we know, SICL is a two conductor transmission line with copper plated through vias which connect the top and bottom ground layers as shown in the layer-wise stack up to form the outer conductor and the sandwiched metallic strip functions as the inner conductor of the this dielectric filled planar coaxial line.The coaxial like radially outward directed E-field vector and concentric H-field in SICL transmission line are confirmed using Ansys HFSS and their field distribution has been shown in Fig. 1.5. To understand the dual-frequency operation with $\pm 90^{\circ}$ phase difference between input and output at the two chosen frequencies, the ABCD matrix of the proposed transmission line is derived.

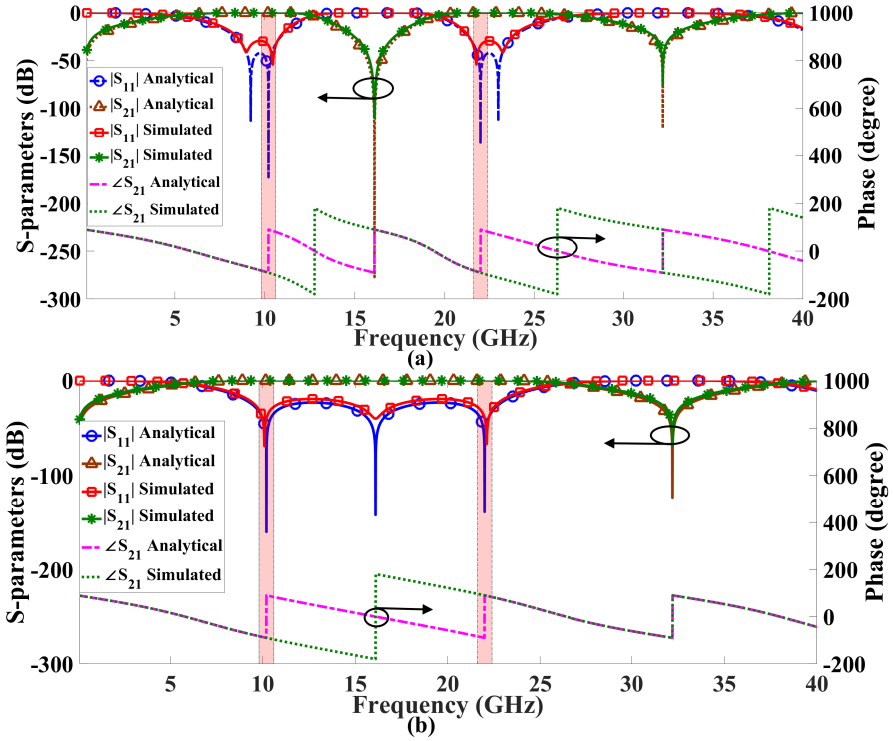

Figure 4.44 : Analytical and simulated S-parameters of the proposed SICL based dual-frequency line (a) Case I: m = n = 1 (b) Case II: m = 2, n = 1.

$$[ABCD]_{\text{overall}} = \begin{bmatrix} 1 & 0 \\ Y_s & 1 \end{bmatrix} \begin{bmatrix} \cos\theta_x & jZ_a \sin\theta_x \\ jY_a \sin\theta_x & \cos\theta_x \end{bmatrix} \begin{bmatrix} 1 & 0 \\ Y_s & 1 \end{bmatrix} \tag{4.18}$$

Where, Y_s is the admittance of the short circuited stub given by $-jY_d \cos\theta_y$. The goal of the proposed SICL transmission line is to act as a quarter-wavelength transformer of desired characteristic impedance at the two chosen frequencies.

The goal of the proposed SICL transmission line is to act as a quarter-wave transformer at two chosen frequencies. To ensure this the ABCD matrix of the proposed transmission line is equated

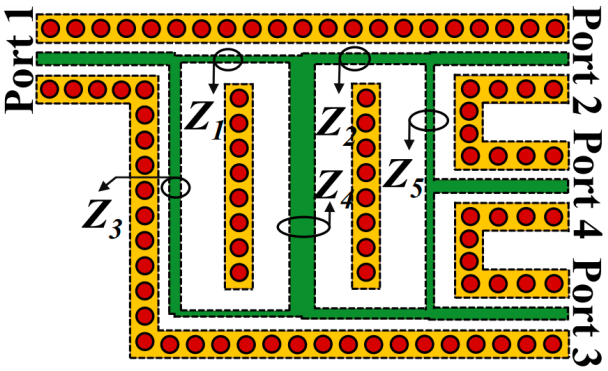

Figure 4.45 : SICL rat coupler with quarter-wavelength transmission lines of characteristic impedance Z_1 = 74.1Ω, Z_2 = 56.7Ω, Z_3 = 52.9Ω, Z_4 = 30.8Ω, and Z_5 = 66.1Ω.

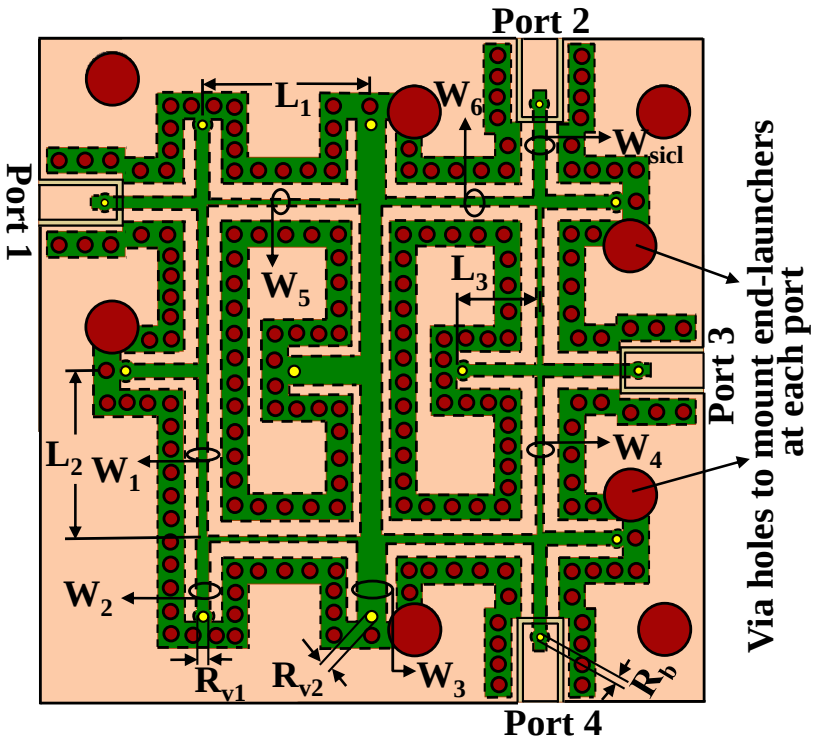

Figure 4.46 : Geometrical layout of the proposed compact dual-wide SICL rat-race coupler with dimensions: L_1 = 6.43mm, L_2 = 6.43mm, L_3 = 3.17mm, R_b = 0.26mm, R_{v1} = 0.4mm, R_{v2} = 0.44mm, W_1 = 0.35mm, W_2 = 0.48mm, W_3 = 1.12mm, W_4 = 0.23mm, W_5 = 0.2mm, W_6 = 0.33mm, W_{sicl} = 0.48mm

with ABCD matrix of a quarter-wave transformer.

$$[ABCD]_{QWTL} = \begin{bmatrix} 0 & Z_o \\ \frac{1}{Z_o} & 0 \end{bmatrix} \tag{4.19}$$

On equating (4.18) and (4.19) the unknown impedances and electrical length of the proposed SICL transmission line are determined as

$$Z_a = \frac{Z_o}{\sin\theta_x}; \quad Z_d = \frac{Z_o \cot\theta_y}{\cos\theta_x} \tag{4.20}$$

$$\theta_x = \frac{m\pi}{1+k}; \quad \theta_y = \frac{n\pi}{1+k} \tag{4.21}$$

where m and n are integers and k is the frequency ratio (f_2/f_1). A three dimensional design curve to determine the unknown impedances Z_a and Z_d of the proposed SICL based dual-band line as a continuous function of Z_o, and frequency ratio is shown in Fig. 4.41. In this work, two configurations based on values of integers m and n of the proposed SICL based dual-band line are examined. In case I, m and n are chosen as 1 and the trigonometric equation (4.20) is solved for a six fixed values of Z_o to determine Z_a and Z_d at various different frequency ratios as shown in Fig 4.42. Similarly, Z_a and Z_d is determined in Fig 4.43 for case II: m = 2 and n = 1. In order to achieve suppression of the third harmonic the short circuited coaxial stub has to be half-wavelength long at $3f_o$. The choice n = 1 in equation (4.21) ensures the proposed short-circuited stub to simultaneously satisfy the dual-band condition and be half-wavelength long at $3.15f_o$ for the suppression of spurious third harmonic. The ABCD parameters of proposed SICL line in equation (4.18) are

Table 4.3 : Analytically computed Z_a and Z_d for k = 2.15 and Z_o = 50 Ω

Parameter	Value	Value	Parameter	Value	Value
	Case I	Case II		Case I	Case II
Z_a	59.60 Ω	54.74 Ω	Z_d	59.60 Ω	79.65 Ω
θ_x	57.01°	114.03°	θ_y	57.01°	57.01°

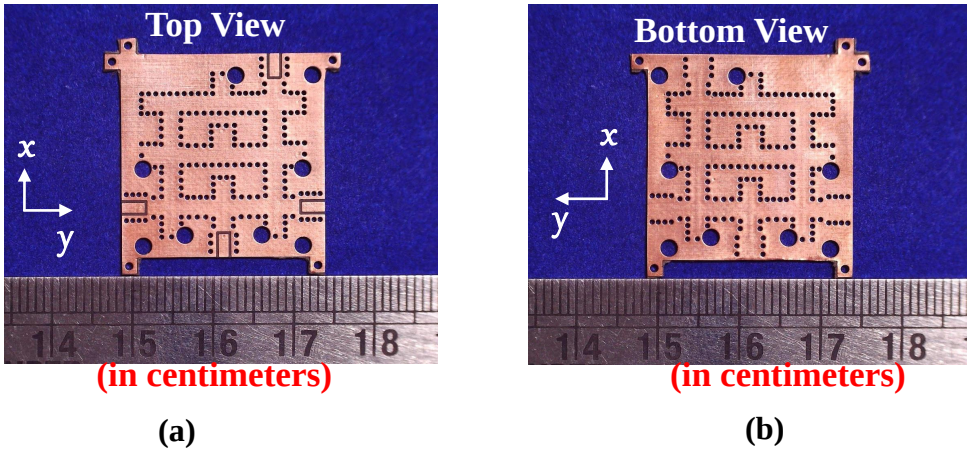

Figure 4.47 : Photograph of the experimental prototype: SICL based dual-broadband Rat-race coupler (a) Top view (b) Bottom view

transformed to S-parameters [130] using MATLAB. The analytically computed S-parameters of the proposed SICL based dual-band line (case I and case II) for a frequency ratio 2.15 with band I and band II centered at 10.2 GHz and 22 GHz respectively are verified by comparison with simulation as shown in Fig. 4.44.

The proposed rat-race coupler utilizes SICL based dual-band transmission line to replace the conventional $\lambda_g/4$ line of rat-race coupler shown in Fig. 4.45 to achieve the required dual-broadband operation. The required Z_a and Z_d are computed from Fig. 4.43 and listed in Table. 4.3 for the frequency ratio 2.15. In the final layout, characteristic impedance of each SICL transmission line of proposed dual-band SICL line is calculated by using the equation (2.9). The required characteristic impedance is realized in the physical layout by selecting the appropriate width of inner conducting strip and outer conductor by using the equation (2.9).

4.5.2 Results and Discussion

The geometrical layout of the proposed dual-broadband coupler in SICL Technology for *X* and *K*-band with dimension is shown in Fig. 4.46. The photograph of the proposed SICL based dual-broadband coupler fabricated using Taconic TLY-5 (ε_r = 2.2, δ = 0.0009) with thickness 0.25 mm for the upper and lower substrate and Taconic FR-28 as prepeg (ε_r = 2.74, tanδ = 0.0014) is shown in Fig. 4.47. The full-wave simulated response generated using Ansys HFSS is confirmed by measuring the S-parameters of proposed prototype using Agilent N5234A vector network analyzer as shown in Fig. 4.48 and 4.49. Measured return loss better than 18.5 dB is observed in band I and II. The frequency band I ranging from 9.38 GHz to 12.28 GHz demonstrates measured amplitude imbalance less than ±0.91 dB and phase imbalance better than ±3.1°. In the band II

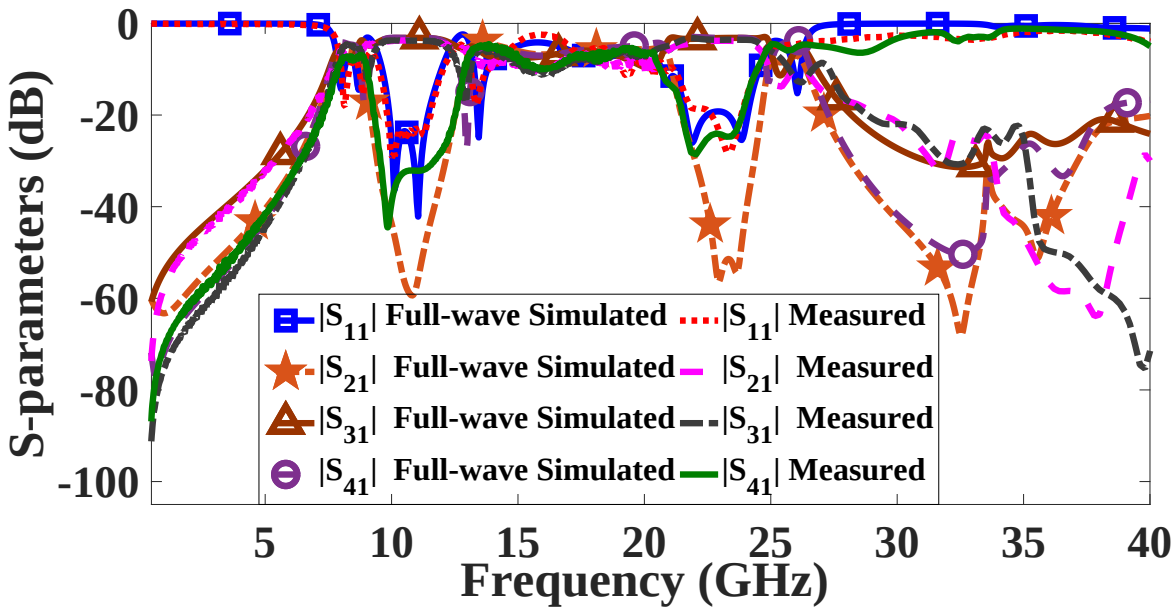

Figure 4.48 : Full-wave simulated and measured S-parameters of the proposed SICL based dual-broadband rat-race coupler with spurious rejection.

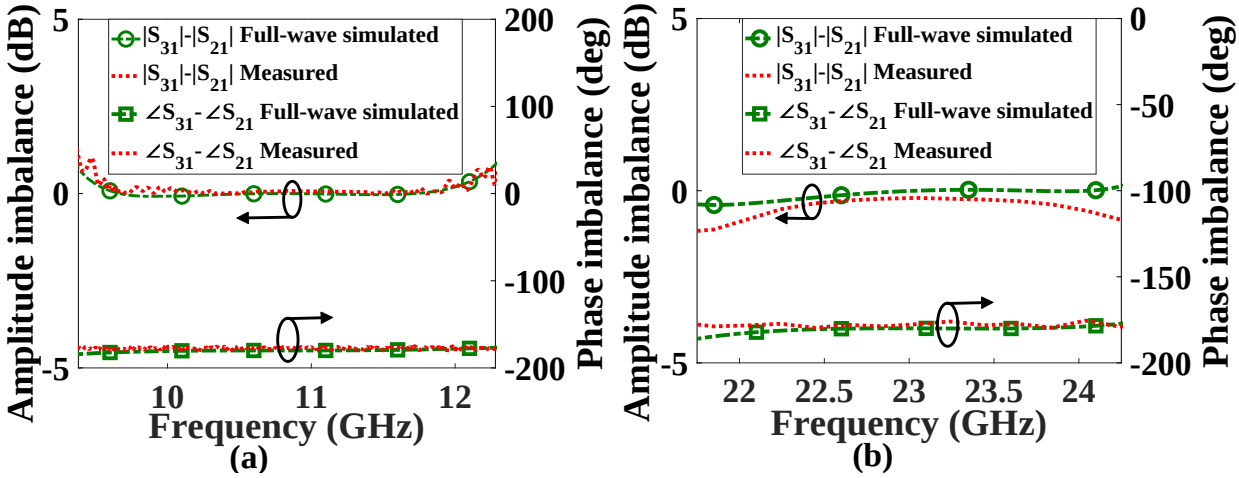

Figure 4.49 : Full-wave simulated and measured amplitude imbalance and phase difference at (a) Band I: *X*-band (b) Band II: *K*-band.

covering the frequencies 21.65 GHz to 24.24 GHz the measured amplitude imbalance is less than ±1.35dB and phase imbalance is ±4.2°. The measured FBW at both bands are 26.69% and 11.28% respectively. The short-circuited planar coaxial stubs along with facilitating dual-band operation also aids in suppressing the third-harmonic and achieves spurious rejection better than 22 dB achieved up to 40 GHz. The proposed SICL coupler covers a lateral area of 21.1 mm × 21.34 mm or equivalently $1.28\lambda_g^2$, where λ_g is guided wavelength at 10.83 GHz. The prominent features of proposed dual-broadband SICL based rat-race coupler in brief are:

1. In the proposed work, a dual-broadband rat-race coupler for *X* and *K*-band is designed in SICL technology with a FBW of 26.69% and 11.28% respectively & offers low amplitude imbalance of

$\pm$1.3 dB and phase imbalance better than $\pm 4.2^{\circ}$ at both the bands.

2. In this work the short circuited coaxial stubs also suppress the third-harmonic of the proposed SICL based rat-race coupler and block the spurious harmonics with rejection level better than 22 dB up to 40 GHz.

3. The proposed dual-broadband coupler in SICL technology is fully shielded by the outer conductor formed by plated vias and top/bottom ground planes. Robust electromagnetic compatibility is attained due to absence of slots on the top/bottom ground planes.

4.6 SICL-BASED WIDEBAND CROSSOVER WITH LOW PHASE IMBALANCE AND GROUP DELAY

This work presents a wideband crossover developed using substrate integrated coaxial line (SICL) technology. The proposed SICL based crossover isolates the two physically overlapping channels by routing the signal in middle conductor of SICL through the transmission line created in the top and bottom ground plane using a metalized blind via. An equivalent model is proposed to study the role of substrate height in the proposed crossover. The design methodology is affirmed by fabricating and testing the experimental prototype. Owing to the non-dispersive nature of SICL line and simplistic design technique with minimal discontinuities the designed crossover demonstrates low peak to peak group delay variation over the entire bandwidth.

4.6.1 Design of SICL line and its transition to GCPW line

The layout of the proposed SICL based crossover is shown in Fig. 4.50. A substrate integrated coaxial line is devised by enclosing a metallic inner conductor between a pair of dielectric substrates. Parallel delimiting vias running along the inner conductor with a bottom and top ground plane form the outer conductor of this planar coaxial line. A metallic strip passing through the lateral vias improve the shielding and enhances the coaxial nature. SICL presents a wideband mono-mode TEM mode propagation similar to its non-planar counterpart, coaxial line. The characteristic impedance of the SICL section is related to its substrate height and width of inner conductor [51]. In Fig. 4.51(a), using full-wave simulator Ansys HFSS the characteristic impedance of the SICL section is determined by fixing the substrate height and varying width of inner conductor and vice versa. From Fig. 4.51(a) for a total substrate height of 1 mm with inner conductor width 0.86 mm the characteristic impedance of SICL is obtained as 50 Ω. The required characteristic impedance of SICL realized by selecting the appropriate width of inner conducting strip and outer conductor can also be verified by using the equation (2.9). SICL to GCPW transition [24, 18, 129, 28, 13] is popularly used to test SICL based components. This transition is realized using a metallic via connecting the inner conductor of SICL to the signal line of GCPW as shown in inset of Fig. 4.51(b). The performance of the transition for different substrate thickness is shown in Fig. 4.51(b). It is observed that in thicker substrates the insertion loss degrades due to increase in parasitics associated with greater height of the blind via. Also the degradation in performance due to surface roughness of blind via will affect more in thick substrates. Hence to maintain low insertion it is preferable to utilize thin substrates

4.6.2 Design and analysis of proposed SICL based crossover

The geometrical layout and 3-dimensional stack up of the proposed crossover is shown in Fig. 4.50. The design of proposed crossover starts with modeling of two channels crossing each other. The first path comprises of 50 Ω SICL section, a transmission line designed in the top ground plane, followed by another SICL line. The SICL line is connected to the transmission line in top ground plane using a vertical blind via. Similarly, the second path consists of 50 Ω SICL line connected to a transmission line in bottom ground which is further fed to an SICL line.

The transmission line designed in bottom and top ground plane are kept compact to preserve the shielded nature of crossover and maintain a small footprint while ensuring good isolation between the channels. An equivalent model of the proposed crossover is shown in Fig. 4.52. The proposed wideband crossover isolates the two physically overlapping symmetrical channels by routing the signal in middle conductor of SICL through the transmission line created in the top and bottom ground plane using a metalized blind via as interconnect. In the overlapping region, the transmission line designed on top/bottom plane is not purely GCPW due to the slots on either side which causes the characteristic impedance to te from 50 Ω. Hence, the central overlapping portion of the transmission line in top/bottom is modeled as an quasi-GCPW line. Further, proper

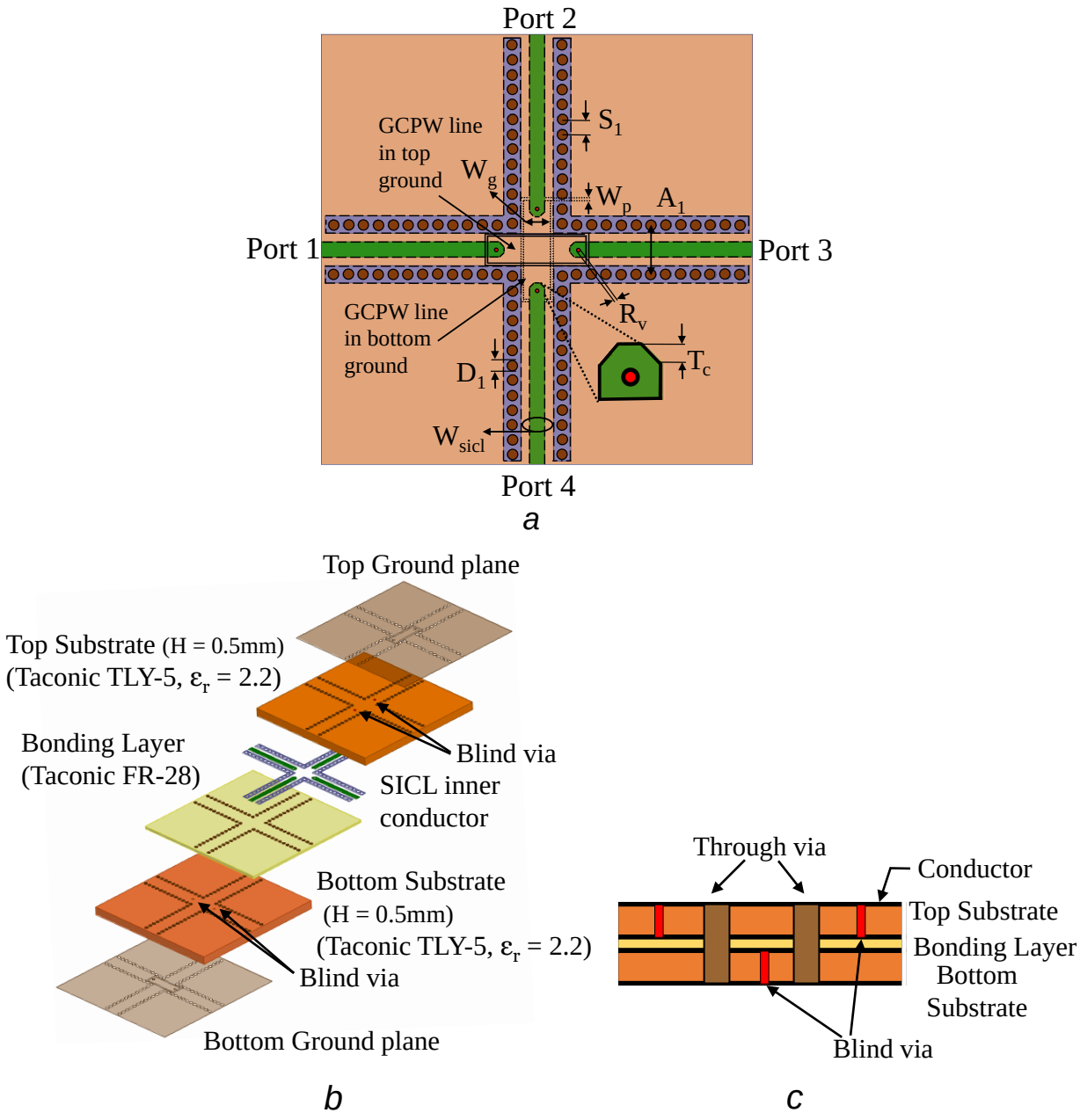

Figure 4.50 : Modeling of proposed SICL based crossover (a) Geometrical layout with dimensions A_1 = 3mm, D_1 = 0.6mm, R_v = 0.2mm, S_1 = 0.9mm, T_c = 0.3mm, W_g = 1.7mm, W_p = 0.13mm, W_{sicl} = 0.86mm (b) 3D stack up (c) Cross-sectional view

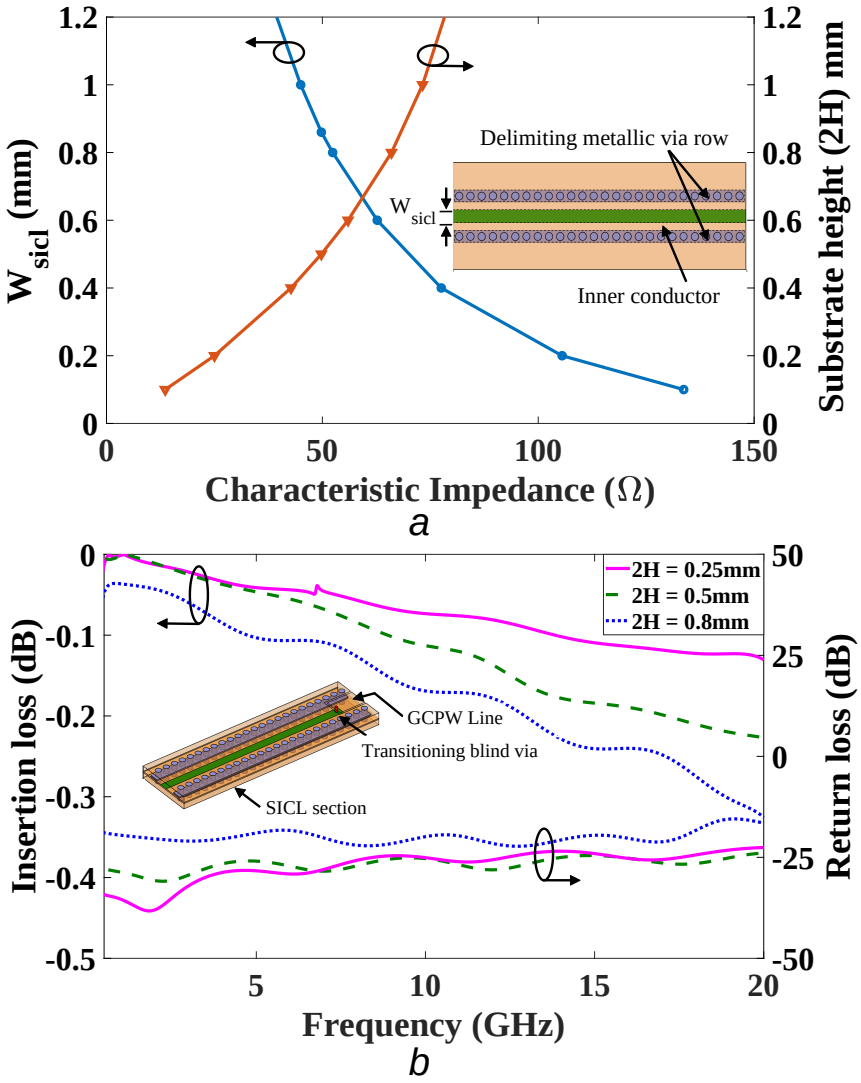

Figure 4.51 : Characterization of SICL transmission line (a) Variation of Z_o with width of inner conductor (W_{sicl}) and height of substrate (b) Performance of SICL to GCPW transition with change in substrate height

design of interconnect between SICL and transmission line in top/bottom plays a crucial role in obtaining the desired characteristics of crossover. This via is modeled using series inductance L_{via} with shunt capacitance C_t and C_b that accounts for capacitive parasitics between top ground plane and via, & inner conductor of SICL section and via, respectively. A capacitance C_g is created due capacitive coupling of blind via with bottom ground plane. The effective inductance contributed by via and its capacitance with top ground is approximated [160] using (4.22) and (4.23).

$$L_{via} = 5.08h\left[\ln\left(\frac{4h}{D_1}\right)+1\right] \tag{4.22}$$

$$C_t = \frac{1.41\varepsilon_r h D_1}{(D_2 - D_1)} \tag{4.23}$$

Where, h is the total height of substrate, D_1 is diameter of blind via, D_2 is diameter of via pad in inches and ε_r is the dielectric constant of the substrate. Tapering the edges of the SICL transmission

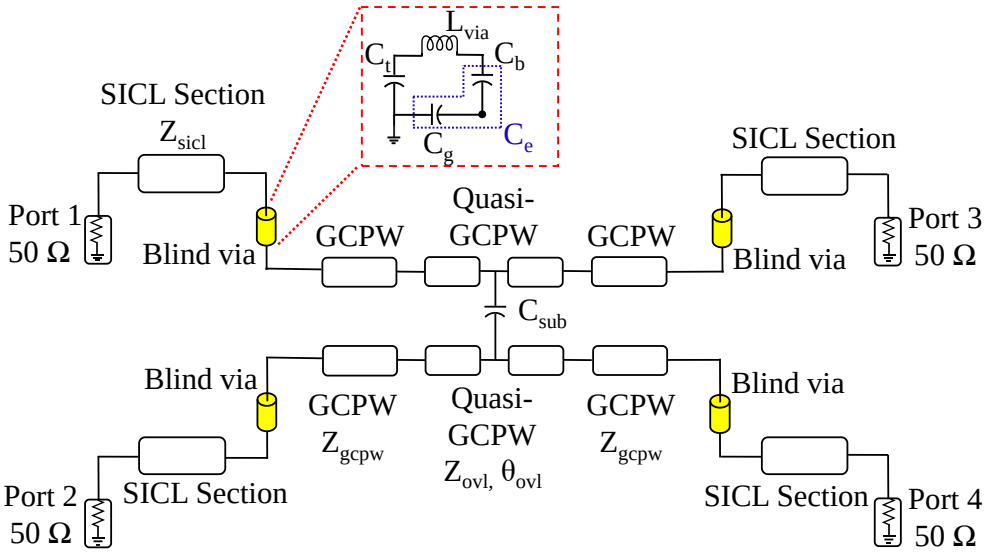

Figure 4.52 : Equivalent model of the proposed SICL based crossover with parameters Z_{sicl} = 50 Ω, Z_{gcpw} = 50 Ω, Z_{ovl} = 62.3 Ω, θ_{ovl} = 32°, L_{via} = 0.3303 nH, C_t = 0.0698 pF, C_e = 0.0623 pF and C_{sub} = 0.032 pF.

line provides increased flexibility in control of parasitics at middle layer and is chosen such the characteristic impedance of blind via ($Z_o = \sqrt{L_{eff}/C_{eff}}$) is close to 50 Ω to achieve good impedance matching between SICL and GCPW line as shown in Fig. 4.54(a). The equivalent capacitance of C_b and C_g is denoted by C_e in Fig. 4.52. The capacitance C_e is calculated as:

$$C_e = \frac{L_{via}}{Z_o^2} - C_t. \tag{4.24}$$

Using the analytically calculated parameters, the circuit simulated performance of the blind via is demonstrated in Fig. 4.53 with return loss better than 20 dB. The characteristic impedance in quasi-GCPW is determined from Ansys HFSS to be 62.3 Ω. A parametric analysis on width of transmission line in top/bottom ground plane (W_g) is carried out in Fig. 4.54 (b) to study return

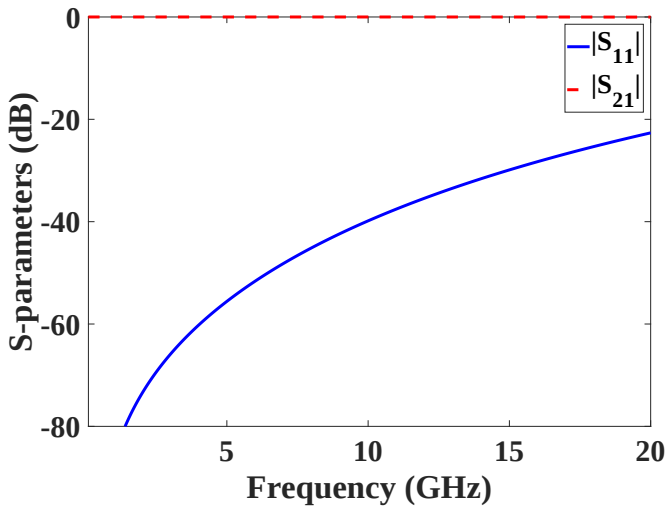

Figure 4.53 : Circuit simulated performance of the blind via

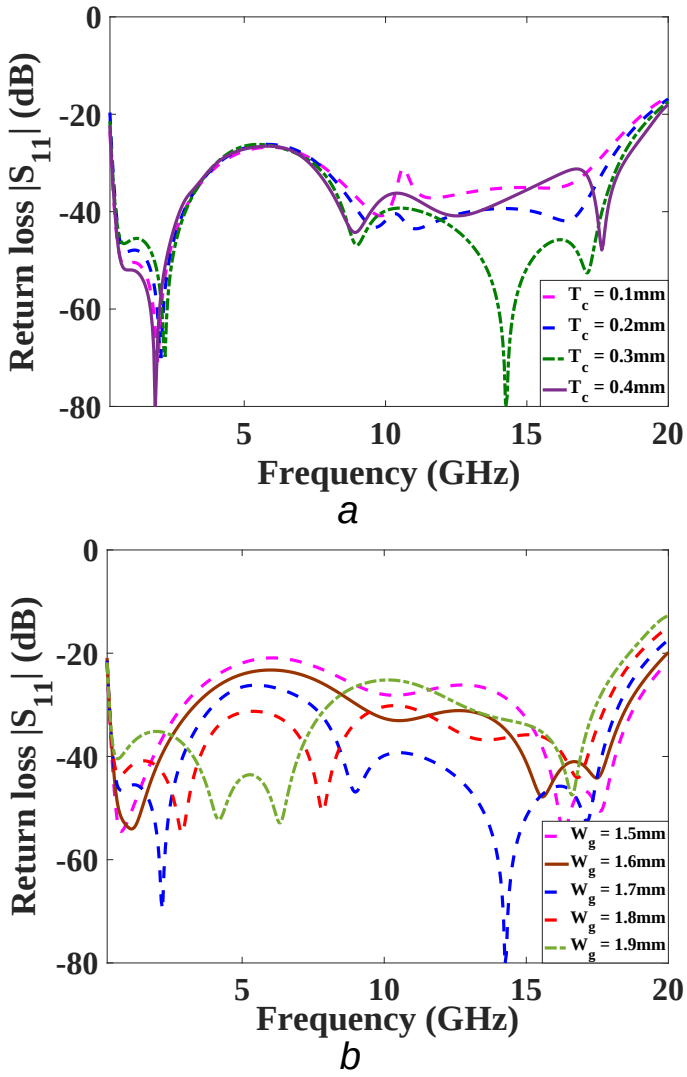

Figure 4.54 : Parametric study of the proposed crossover (a) Dependence of return loss on T_c (b) Variation in width of signal line in top/bottom transmission line (W_g)

loss characteristics of the proposed crossover. It can be seen that for trace width 1.7mm and signal to ground gap of 0.13 mm, the 50 Ω GCPW line along with a central 62.3 Ω quasi-GCPW transmission line maintains good impedance matching up to 20 GHz. The capacitance C_{sub} indicates coupling between the overlapping GCPW transmission lines in top and bottom ground plane. The value of C_{sub} is controlled by the height of substrate, dielectric constant and area of overlap between top and bottom GCPW lines. It is determined that with increase in height of substrate, C_{sub} decreases resulting in improvement of isolation between both the paths, on the other hand the insertion loss degrades due to increase in parasitics with blind via. The same has been confirmed using a full-wave simulator by varying substrate height as shown in Fig. 4.55. Hence, this study deduces a trade off between insertion loss and isolation with height of the substrate. The performance of proposed crossover evaluated through its circuit model using ADS software is shown in Fig. 4.56 . In the proposed design, the total substrate height is chosen as 1 mm to achieve insertion loss less than 0.7 dB and isolation better than 19 dB through out the bandwidth. The TEM mode of SICL is advantageous in feeding in the TEM based quasi-GCPW transmission line to achieve a wide bandwidth. The upper bound on operating frequency in the proposed SICL based crossover is mainly dependent on the performance of interconnect and capacitive coupling

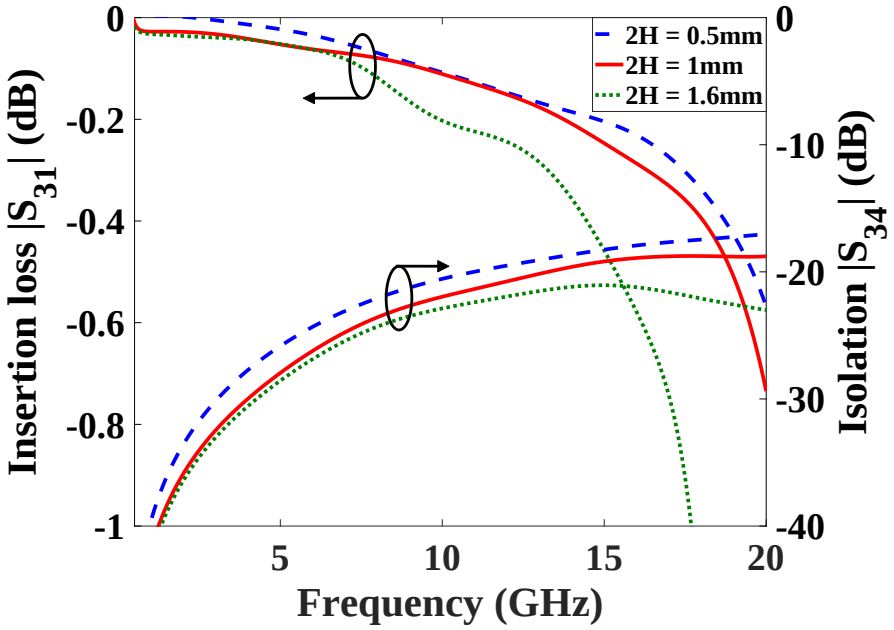

Figure 4.55 : Investigation on characteristics of proposed crossover with change in total height of substrate

between overlapping transmission lines in top & bottom ground plane.

4.6.3 Results and Discussion

The proposed SICL based crossover is fabricated using a pair of low loss Taconic TLY-5 (ε_r = 2.2, tanδ = 0.0009) substrate each of thickness 0.508 mm, which are bonded using Taconic FR-28 prepreg (ε_r = 2.74, tanδ = 0.0014). The physical layout of the proposed configuration with dimensions is depicted in Fig. 4.50. Photograph of the fabricated prototype's top and bottom view

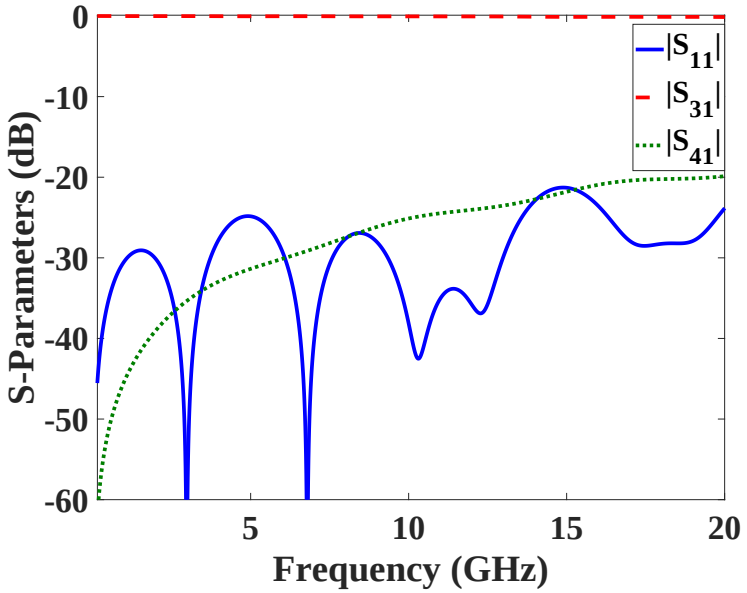

Figure 4.56 : Circuit simulated performance of proposed SICL based crossover

Table 4.4 : Comparison of proposed SICL based crossover with state of the art crossovers

Ref.	Technique	Insertion loss (dB)	Isolation (dB)	Peak group Delay / Deviation (ns)	Bandwidth (GHz)	Phase compensation
[145]	Cascading BLC	0.5	20	13/1	2.2 to 3.1	No
[146]	Cascoding BLC	1	15	1.5/0.1	0.735 to 1.265	-
[147]	Parallel coupled lines	1	12	1/0.4	2.19 to 2.82	-
[148]	Microstrip to CBCPW transition	1	20	-/-	0.1 to 6	-
[149]	Microstrip to slotline transition	1.6	15	0.4/0.1	4 to 8	-
[150]	Microstrip with DGS	0.75	25	-/-	0 to 10	Yes
[151]	Microstrip to CPW transition	1.1	15	0.2/0.08	3.1 to 11	-
[152]	Microstrip to semi-CPW transition	1 1	23.3 18.9	-/- -/-	0 to 10 0 to 10	Yes Yes
[153]	Microstrip ring resonator & circular patch	0.5	18	0.7/0.25	2.15 to 3.35	-
[154]	Square Patch	1	12	0.3/0.06	5.15 to 5.85	-
[155]	Slotted Circular Patch	1	13	0.6/0.1	2.11 to 2.68	-
[156]	Sierpinski fractal	1	17	0.85/0.1	2.28 to 2.52	-
[157]	SIW	0.25*	20	-/-	10.6 to 14	-
[158]	SIW	2	18	-/-	27.4 to 32.4	-
[162]	SIW	0.9	17	-/-	32 to 38	-
[164]	CBCPW slot coupled hybrid	0.5*	15	-/-	3 to 10	-
[163]	Stripline	-	28	-/-	1 to 4	Yes
[165]	Cascaded slot coupled couplers	0.2*	22.4	-/-	5 to 6.5	-
[166]	Double slot coupled transitions	1.3	25	-/-	3.1 to 10.6	-
TW	SICL	**≤0.67 dB up to 10 GHz** **≤1.2 dB up to 20 GHz**	**≤25.4 up to 10 GHz** **≤19 dB up to 20 GHz**	0.21/0.04	0.2 to 20	No

*: Simulated data, TW: This work, BLC: Branch line coupler, CBCPW: Conductor backed coplanar waveguide

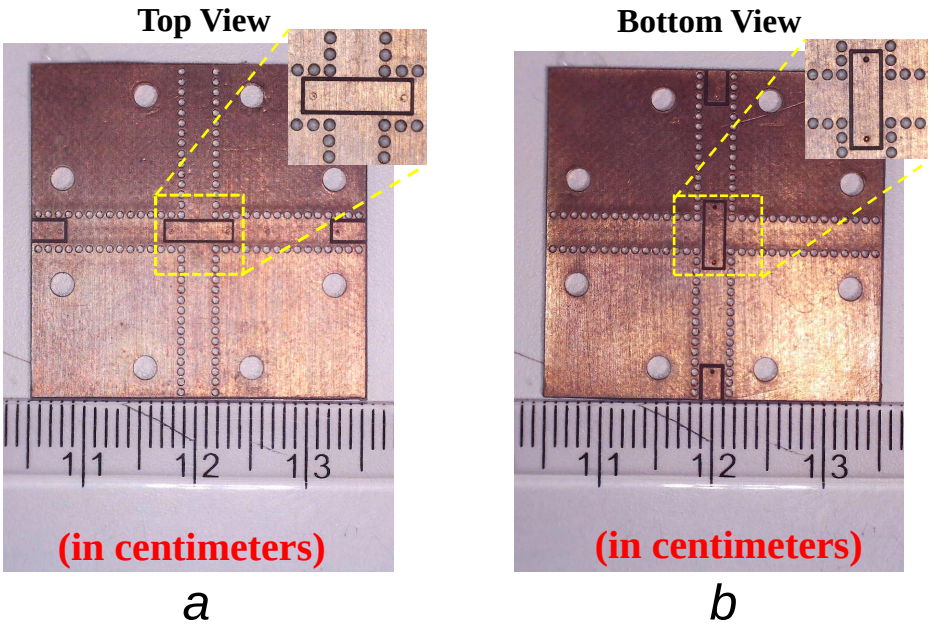

Figure 4.57 : Photograph of the fabricated SICL based crossover (a) Top view (b) Bottom view

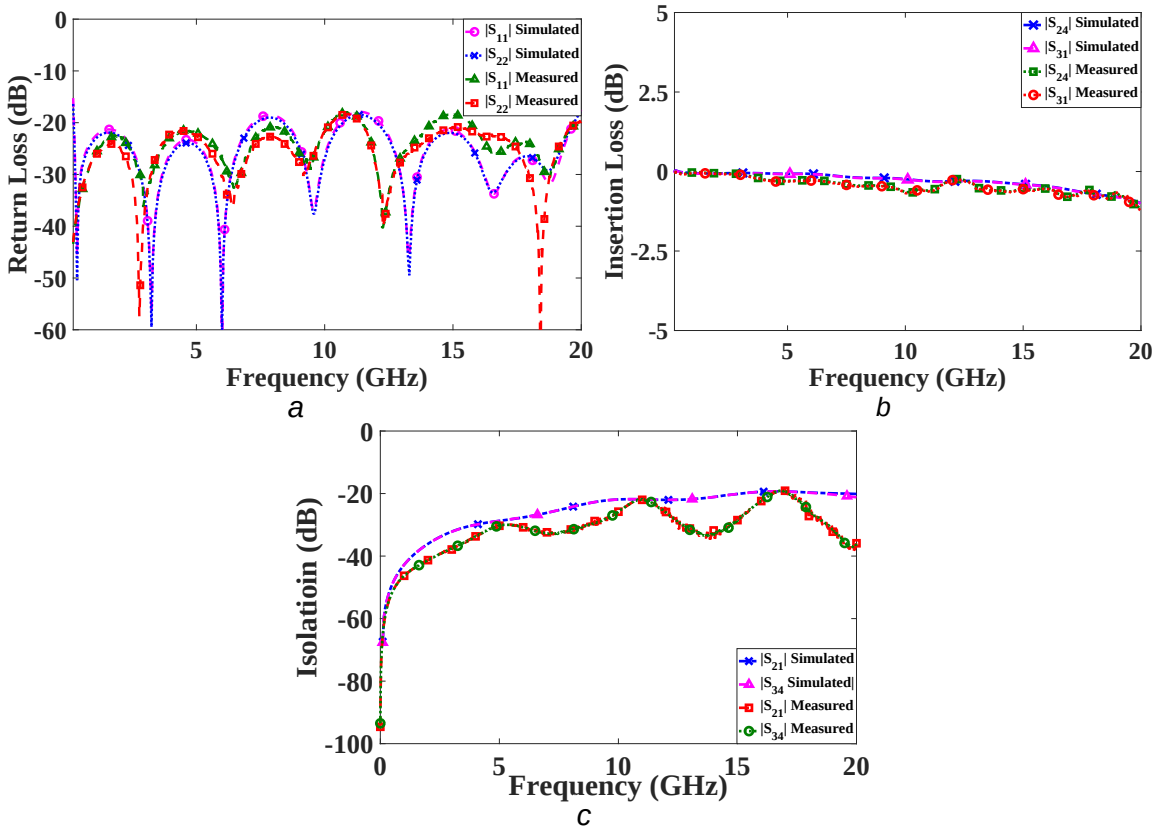

Figure 4.58 : Measured and full-wave simulated performance of the proposed crossover (a) Return loss (b) insertion loss (c) Isolation

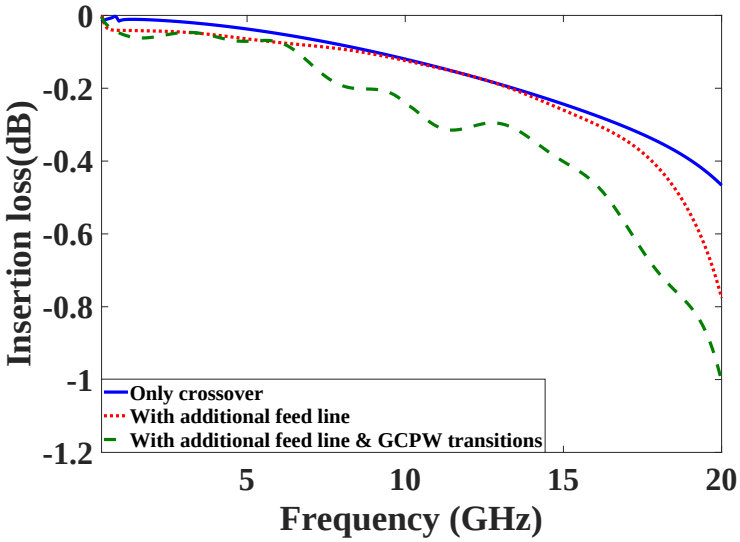

Figure 4.59 : Effect on insertion loss due to additional feed lines and GCPW transition

is shown in Fig. 4.57. The proposed SICL crossover is measured with four SMA end-launchers using Agilent E5071C vector network analyzer. The tested SICL crossover exhibiting wide-band nature with better than 18 dB return loss and less than 1.2 dB insertion loss from 0.2 to 20 GHz (insertion loss less than 0.67 dB and isolation better than 25.4 dB up to 10 GHz) is in good agreement with predicted full-wave results as illustrated in Fig. 4.58. To facilitate measurement of the proposed prototype, four SICL to Grounded coplanar waveguide (GCPW) transitions are used. Further, 10mm additional feed length at all four ports are maintained to accommodate SMA end launchers without any overlap. The measured insertion loss of the fabricated SICL crossover also takes into account these additional SICL-GCPW transitions and 10mm long SICL transmission lines at each port. However, in practical applications such as an SICL based transceiver system the

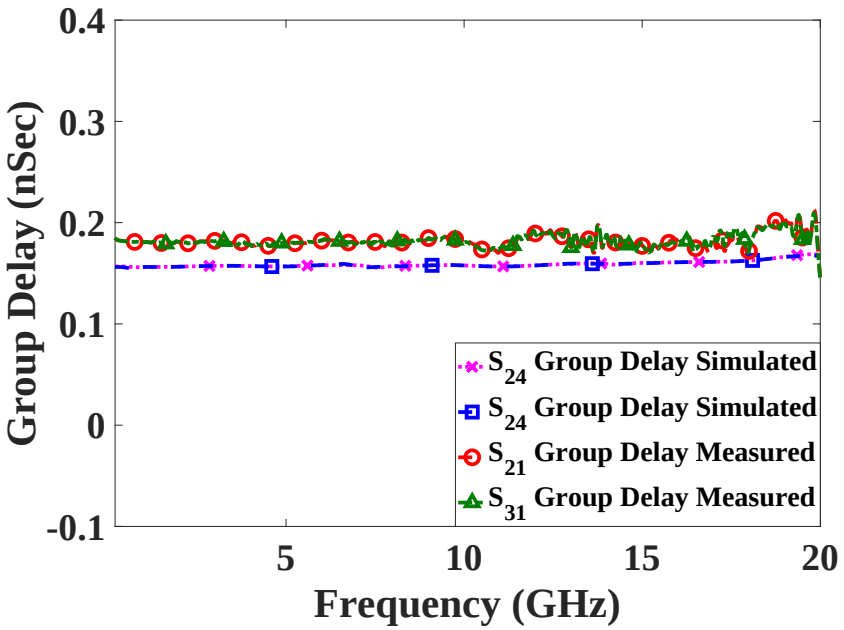

Figure 4.60 : Measured and full-wave simulated S_{24} and S_{31} group delay

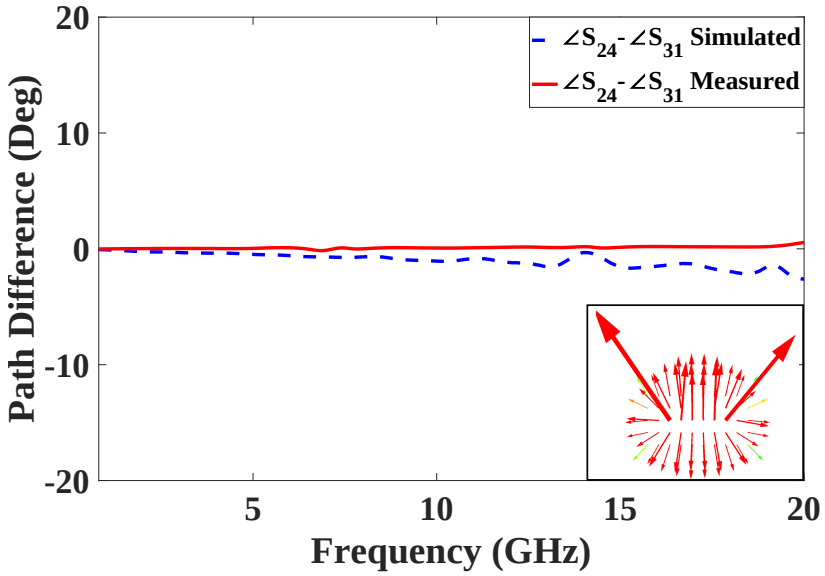

Figure 4.61 : Comparison between measured and full-wave simulated path difference between channel 1 and 2 of the proposed crossover

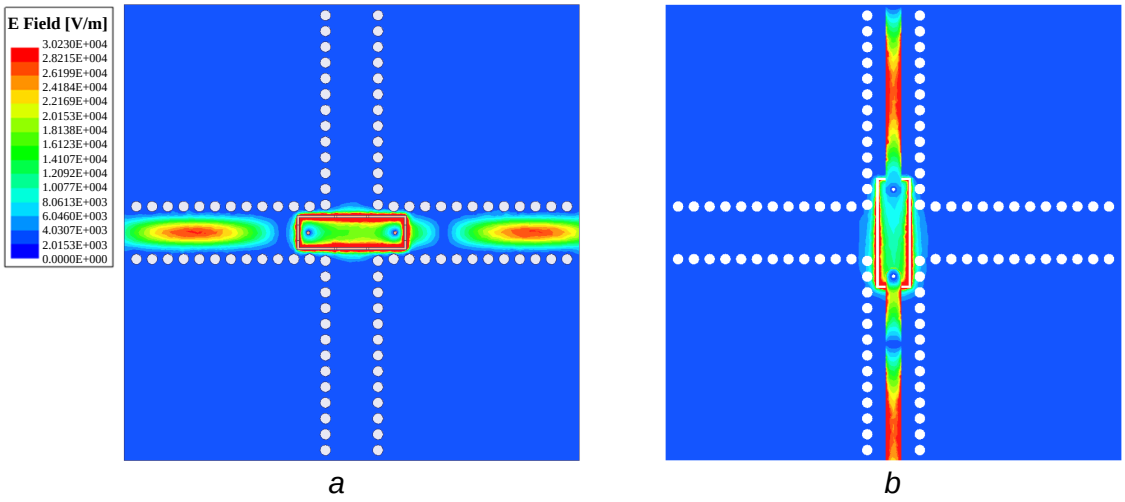

Figure 4.62 : Magnitude of electric field in (a) Inner conductor and top ground plane (path 1) (b) Inner conductor and bottom ground plane (path 2)

requirement of additional SICL to GCPW transitions and feed length would be eliminated since the proposed crossover is integrated with the follow-up planar components of the front-end of transceiver. In Fig. 4.59 the effect on insertion loss due these interconnects have been illustrated through full-wave simulation. The insertion loss of only crossover without any additional feed line and transitions is better than 0.46 dB up to 20 GHz. It is to be noted the additional feed length and transitions are required only to test the component individually and losses due to them wouldn't be accounted when used in a system.

A distortion less performance is achieved using the proposed design principle as it has minimal discontinuities with non-dispersive behavior of SICL to achieve a low measured group delay variation of 0.04 ns with peak group delay of 0.21 ns is shown in Fig. 4.60. The slight inconsistency between measured and simulated results can be attributed to the fabrication

tolerances and air gap in bonding the two substrate layers. Crossovers are required in design of butler matrix, which is a feeding network used to steer the beam of high gain antennas. It is crucial to design crossover with low phase difference between output ports to accurately steer the beam in the intended direction. Due to the symmetrical design, a low phase difference of less than $\pm 2.45^{\circ}$ measured between the channels up to 20 GHz (less than $\pm 1^{\circ}$ up to 10 GHz) is achieved as shown in Fig. 4.61 . The radially outward vector electric field across SICL section depicted in inset of Fig. 4.61 demonstrates field distribution similar to traditional coaxial [129, 28] confirming SICL to be it's planar counterpart. The electromagnetic robustness of the self packaged SICL structure obtained from an outer conductor formed by shielding metallic vias and both ground planes is shown in Fig. 4.62. It is observed that both the channels are completely isolated from each other with negligible electric field outside the via wall, making the proposed design suitable for compact and densely integrated systems. The performance of the designed SICL crossover is compared with an exhaustive literature of wideband and low group delay crossovers in Table 4.4. It can be observed from [145, 146, 147, 148, 149, 150, 151, 152, 153, 154, 155, 156, 157, 158, 162, 164, 163, 165, 166] that many novel techniques have been proposed to design UWB crossovers with low group delay to achieve a maximum operational bandwidth from DC up to 11 GHz. The proposed SICL crossover achieves a bandwidth up to 20 GHz with low group variation in the operating band without any additional phase compensation circuit. The proposed crossover covers a lateral area of $0.3\lambda_g \times 0.3\lambda_g$, and volume of 0.0041 λ_g^3, where λ_g is guided wavelength at 10 GHz.

The prominent features of proposed SICL wideband crossover are discussed in brief as below:

1. **Wide bandwidth:** The measured results show isolation between channels are more than 19 dB with better than 18 dB return loss and less than 1.2 dB insertion loss from 0.2 to 20 GHz. As shown in comparison table the proposed SICL crossover is the only crossover to best of authors knowledge having wide bandwidth to cover *L*, *S*, *C* and prominent higher *X* and K_u bands simultaneously. Further, the TEM mode of SICL is advantageous in feeding in the TEM based quassi-GCPW transmission line to achieve a wide bandwidth.

2. **Low group delay**: Owing to the non-dispersive nature of SICL line and simplistic design technique with minimal discontinuities the designed crossover demonstrates low peak to peak group delay variation, less than 0.04 ns over the entire bandwidth which is lowest in the literature to best of authors knowledge.

3. **Low path difference:** Crossover is an integral component in design of butler matrix for design of beam steering of high gain antennas. It is crucial to design a crossover with low phase difference between output ports to accurately steer the beam in the intended direction. The proposed crossover due to its symmetric design provides low path difference of less than $\pm 2.45^{\circ}$ up to 20 GHz ($\leq \pm 1^{\circ}$ up to 10 GHz), as a result the requirement for additional phase compensation technique is eliminated.

4. **Compact:** The proposed crossover implemented in SICL technology is an attractive candidate in RF-front end architecture where small form factor is preferred for installation in modern hand-held devices and access points.

5. **Shielded and self-packaged structure:** The electromagnetic robustness of the self-packaged SICL structure obtained from the outer conductor formed by shielding metallic vias and both ground planes helps in maintaining excellent isolation in densely integrated systems.

   The crossover proposed in [148], the first channel comprises of microstrip and CB-CPW line, whereas the second channel consists of microstrip line connected to CB-CPW line using

Table 4.5 : Comparison of proposed SICL based wideband crossover with a microstrip crossover

	[148]	Proposed work
Technique	Microstrip to GCPW	SICL based crossover
Insertion loss	< 0.4 dB$^{\#}$ at 6GHz	$\leqq 0.36$ dB* at 6GHz $\leqq 1.2$ dB* at 20GHz
Isolation	> 20 dB at 6GHz	$\geqq 31$ dB*at6GHz $\geqq 19$ dB*at20GHz
Peak group delay/ Group delay deviation	$--$	0.04/0.2 ns
Bandwidth	0.1 to 6GHz	0.2 to 20GHz
Phase compensation	Not shown	Not required
Phase difference between output ports	Not shown	$\leq 0.58^{\circ}$ at 6GHz $< 2.45^{\circ}$ at 20GHz
Shielded and Self-packaged	No	Yes

metallic via holes. Due to different channel type a phase difference is created between the output ports. To overcome this problem, in [152] extra slots are etched in overlapping portion of the transmission lines to maintain a phase difference less than 5^{o} between output ports at 10 GHz. Additional delay lines are used in [150] to externally compensate the phase difference created due to asymmetrical paths in the crossover. Utilization of additional slots and delay lines increase the complexity and lateral area of the design. The proposed SICL based crossover benefits from the completely symmetrical channels and eliminates the need for additional slots or delay lines. The measured results of fabricated prototype indicate low phase difference between output ports up to 20 GHz . But, in [148], the crossover designed using microstrip to GCPW transition operates only up to 6 GHz. Semi open-structures such as microstrip [148, 149, 150, 151, 152, 153, 154, 155, 156] are lossy at higher frequency and have shown to demonstrate a maximum bandwidth up to 10 GHz as shown in Table 4.4. Poor lateral shielding by stripline [163] and narrow-monomode bandwidth of SIW structure [157, 158, 162] makes it unsuitable for design of compact wideband crossovers covering lower frequency bands like L, S, C and higher bands like X and Ku simultaneously. The proposed SICL based crossover demonstrates operability up to 20 GHz in a compact form factor.

4.7 DESIGN OF A WIDEBAND WILKINSON POWER DIVIDER FOR K_U-BAND

Power dividers are widely used in microwave/ millimeter-wave systems for design of a variety of applications such as in balanced amplifiers, inphase-quadrature (IQ) modulators, and antenna arrays. The popularly used T and Y junction based power divider through provides required power division ratio, but is not matched at all ports and requires additional quarter-wave transformers. An attractive alternative to this is the resistive power divider which is matched at all ports although 50% of the input power is dissipated through resistors. Resistive power dividers tend to be lossy but are compact and hence find wide applications in IC based design where an additional amplifier is usually incorporated to compensate for the power loss. Wilkinson power dividers provide good impedance matching at ports with low loss and very high isolation with various power combing/division ratios. Since all passive components are used it is also reciprocal in nature.

In this work the modeling of an SICL based wilkinson power divider for wide band applications is explored. The layout of proposed two-stage Wilkinson power divider in substrate integrated coaxial line is shown in Fig.4.63. SICL technology is realized using two layers of double side copper clad substrates. A inner conducting strip sandwiched between the two dielectric substrates with bottom and top ground plane acts as the inner conductor of this coaxial line and the delimiting vias along the inner conductor along with bottom and top grounds plane form the outer conductor. The proposed design starts with two-sections of Wilkinson power divider each of characteristic impedance Z_{s1} and Z_{s2} respectively. The characteristic impedance Z_{s1} = 79.78 Ω and Z_{s2} = 55.2 Ω of the proposed two-stage wilkinson power divider is determined through optimization in ADS simulator for a wide-bandwidth with equal power division and high isolation. An isolation resistor is utilized at the end of each quarter-wavelength section with resistance R_1 and R_2 respectively. Since the conducting strip is sandwiched between the two dielectric strip the isolation resistor cannot be mounted directly. To facilitate the connection of resistor on to each stage of the proposed wilkinson power divider, a blind via connecting the middle conducting to strip to GCPW pads created on the top plane is utilized.

The fabricated experimental prototype of the proposed wideband wilkinson power divider is shown in Fig. 4.64. Standard PCB fabrication is employed to developed the proposed prototype with a couple of low loss Taconic TLY-5 (ε_r = 2.2, tanδ = 0.0009) substrate each of thickness 0.254 mm, which are bonded using Taconic FR-28 prepreg (ε_r = 2.74, tanδ = 0.0014). The three-port wideband SICL based power divider comprises of two GCPW pads connected to the middle layer using blind vias to facilitate the mounting of chip resistors. Techdia's 100Ω and 200Ω resistors are carefully soldered onto the GCPW pads as shown in Fig. 4.64 to function as isolation resistors. The proposed SICL based wilkinson power divider is measured with four Rosenberger SMA end-launchers (32K243-40ML5) using Agilent E5071C vector network analyzer. The experimentally verified SICL based wilkinson power divider prototype supports wide-bandwidth with return loss better than 13 dB which very well conforms with the expected full-wave results as illustrated in Fig. 4.65. In this work three

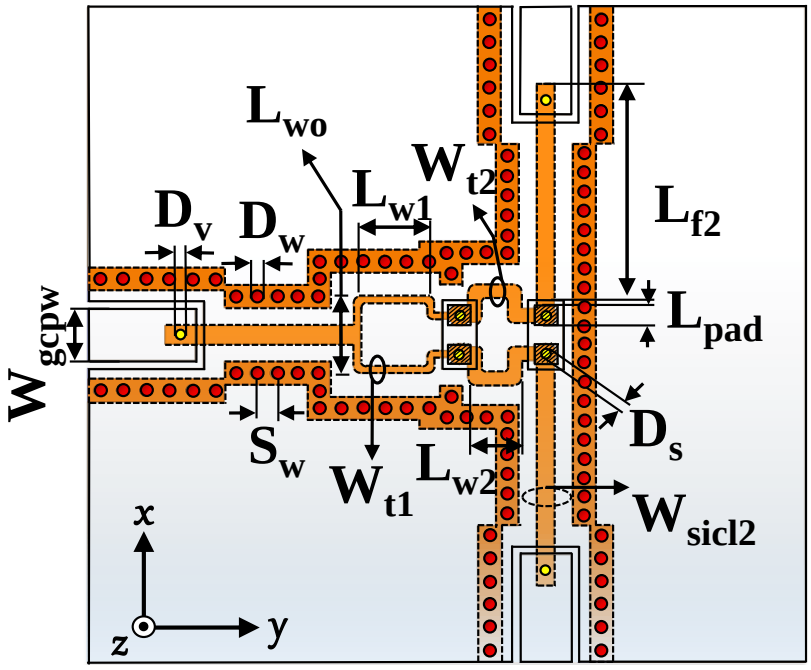

Figure 4.63 : Geometrical layout of the proposed two-stage SICL based Wilkinson power divider.

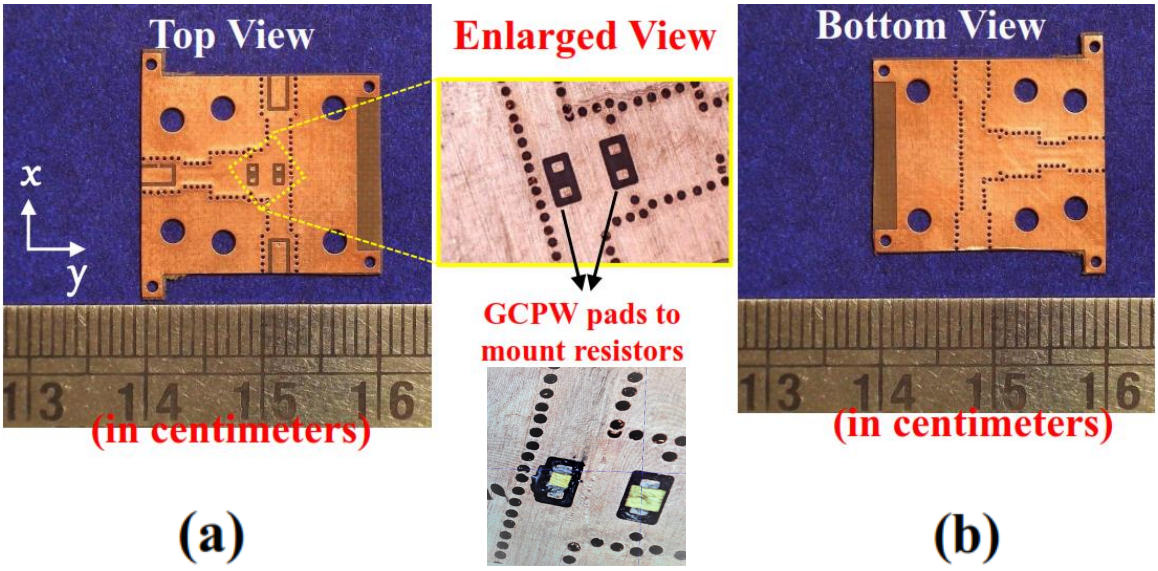

Figure 4.64 : Photograph of the fabricated compact SICL based wilkinson power divider

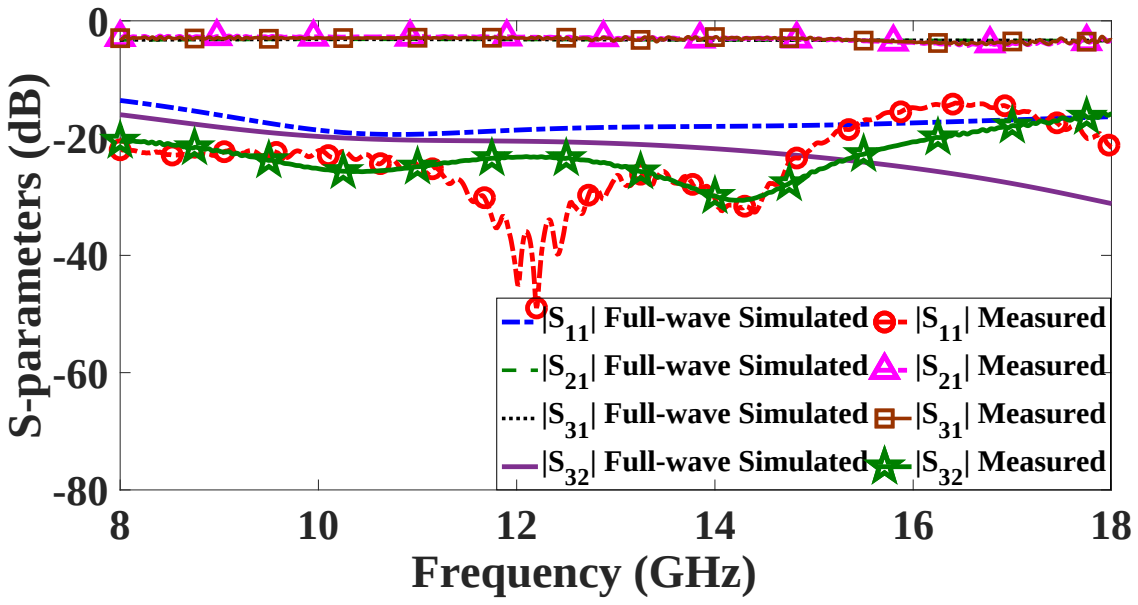

Figure 4.65 : Comparison between the full-wave simulated and measured S-parameters of the proposed SICL based wilkinson power divider

SICL to GCPW transitions are used to mount the end-launchers, and feed length of 5.5mm at all four ports are ensured to mount the SMA end launchers without any overlap. Owing to the resistor network in the proposed power divider an isolation better than 14 dB is obtained between the output port over a wide-bandwidth of 8 GHz to 18 GHz. A low phase difference of 0.3° and amplitude imbalance of 2.2 dB is recorded over the wide-bandwidth of 8 GHz to 18 GHz as shown in Fig. 4.66. The deviation between measured and simulated results can be caused due to the, errors in mounting the SMD resistor, fabrication tolerance and irregular bonding of two substrate layers. The proposed SICL based wilkinson power divider

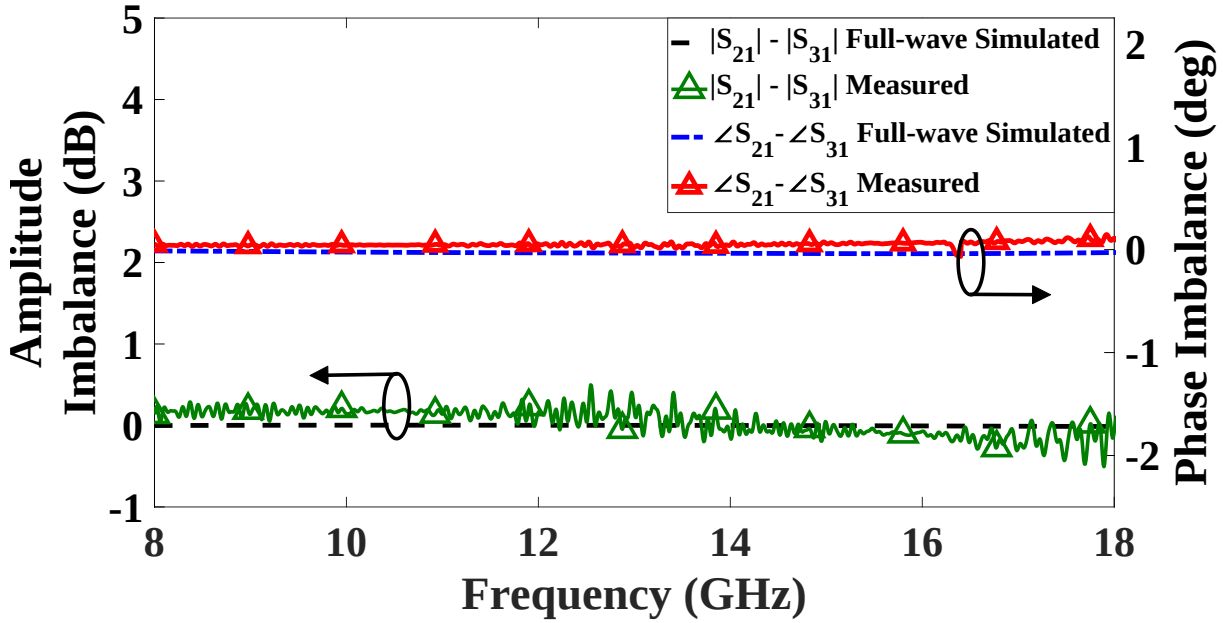

Figure 4.66 : Measured and full-wave simulated Amplitude and Phase imbalance in proposed SICL based wilkinson power divider

demonstrates robust electromagnetic shielding contributed by the outer conductor formed by the lateral vias and top/bottom ground planes of the planar coaxial line . Further it covers a lateral area of only 3.82mm $\times$ 6.93mm or equivalently $0.25\lambda_g \times 0.45\lambda_g$, where λ_g is guided wavelength at 13 GHz.

4.8 CONCLUDING REMARKS

This chapter begins with the discussion on two SICL based wideband baluns for *K*-band applications. The proposed SICL based planar balun operates for a frequency range 17.9 GHz to 26.85 GHz with low amplitude and phase imbalance. The planar SICL balun occupying a lateral footprint of only $0.73\lambda_g \times 0.75\lambda_g \times 0.05\lambda_g$ is fabricated and experimentally validated. The second balun demonstrated in this chapter is a folded wideband balun occupying only 58% lateral area as compared to the proposed planar SICL balun. In both the proposed configurations, lateral vias along with top and bottom ground plane form a shield to prevent unwanted coupling with neighboring circuits, thereby exhibiting good electromagnetic compatibility. The next work deals with the design and development of SICL based dual-band balun operating at 6 GHz and 28 GHz aimed to cover the 5G microwave and millimeter-wave bands simultaneously. The proposed dual-band balun realised using open-ended coaxial stubs is analyzed through the electric field distribution and verified by circuit and full-wave simulated S-parameters. The experimental validation through measurement of fabricated prototype indicated that the proposed dual-band SICL balun covers a frequency range of 5.1 GHz to 6.3 GHz and 26.5 GHz to 27 GHz magnitude imbalance better than $|S_{21}| - |S_{31}| = \pm 1.5$ dB and phase imbalance better than $\angle S_{21} - \angle S_{31} = \pm 2.8^\circ$. The compact form factor and low-loss property of SICL technology makes the proposed dual-band balun a befitting option to deploy in millimeter-wave range.

The design and analysis of a compact SICL based quadrature hybrid with controllable

harmonic rejection is demonstrated. Performance of the proposed quadrature hybrid is experimentally verified up to 20 GHz and found to be in accordance with the simulation. Further, the dependence of transmission zero on the length of open-ended stub is analyzed and verified through simulation. The designed quadrature hybrid achieves a compact size of $0.10\lambda_g^2$ with 12.24% fractional bandwidth.

An SICL based dual-broadband millimeter-wave rat-race coupler using planar coaxial stubs has been realized and verified in this work. The range of realizable frequency ratios for the proposed rat-race coupler are determined analytically and fabricated rat-race coupler experimentally verified achieves FBW of 26.69% and 10.41% centered at 10.83 GHz and 23.15 GHz respectively. The proposed dual-broadband SICL rat-race coupler having low amplitude and phase imbalance with spurious rejection better than 22 dB up to 40 GHz is suitable for practical applications.

The working principle and experimental validation of wideband SICL based crossover have been demonstrated in this chapter. The designed interconnect facilitates in routing the two signal paths independently by efficiently using the top and bottom ground planes to provide an excellent isolation between the overlapping paths. The presented SICL-based crossover with wide unimodal bandwidth works from 0.2 GHz to 20 GHz covering *L*, *S*, *C* bands and other prominent higher *X* and Ku bands simultaneously. An equivalent model of the crossover is developed to investigate the effect of substrate height and demonstrate the trade off between insertion loss and isolation. An insertion loss less than 1.2 dB and isolation better than 19 dB has been affirmed in the entire operating bandwidth of $0.2-20$GHz (insertion loss less than 0.67 dB and isolation better than 25.4 dB up to 10 GHz.) Further, due to the non-dispersive nature of SICL and minimal discontinuities in the design provides a distortion less performance with a low group variation of 0.04 ns and peak group delay of 0.21 ns. The symmetric design without any additional slots aids in the low path difference of less than $\pm 2.45^\circ$ up to 20GHz ($\leq \pm 1^\circ$ up to 10GHz) without any requirement for additional phase compensation. Utilisation of wideband monomode TEM propagation of nondispersive SICL promotes the use of various microwave/millimetre components for beamforming networks and transceiver system.

Finally the design and fabrication of wideband branch-line couplerand two-stage Wilkinson power divider covering the entire *Ku*-band is discussed in detail.

Overall this chapter discusses the design principles to develop SICL based three and four-port networks with wide-bandwidth, dual-band functionality and wide out of band rejection. The superior integration capability of SICL with planar circuits and robust electromagnetic shielding motivates the use of proposed SICL technology for compact form factor to design exceptional front-end communication system. The detailed study carried out here helps to explore new three and four-port networks with enhanced functionalities towards the development of six-port network.

...